Thermodynamics of sea ice phase composition revisited

Martin Vancoppenolle, Gurvan Madec, Max Thomas, Trevor J Mcdougall

Thermodynamics of sea ice phase composition revisited

Martin Vancoppenolle[1], Gurvan Madec[1], Max Thomas[2], Trevor J. McDougall[3]

[1]Sorbonne Université, LOCEAN-IPSL, CNRS/IRD/MNHN, Paris, France
[2]University of East Anglia, Norwich, UK
[3]University of New South Wales, Sydney, Australia

Key Points:

- Revisit sea ice phase composition from observational and theoretical sources
- Quantify uncertainties in brine salinity and mass fraction
- Propose sea ice phase equations with solid minerals that are compatible with international standards

Corresponding author: Martin Vancoppenolle, martin.vancoppenolle@locean-ipsl.upmc.fr

Abstract

Pure ice, brine and solid minerals are the main contributors to sea ice mass. Constitutional changes with salinity and temperature exert a fundamental control on sea ice physical, chemical and biological properties. However, current estimation methods and model representations of the sea ice phase composition suffer from two limitations – in a context of poorly quantified uncertainties. First, salt minerals are neglected. Second, formulations are inconsistent with international standards, in particular with the International Thermodynamic Equation of Seawater (TEOS-10). To address these issues, we revisit the thermodynamics of the sea ice phase composition by confronting observations, theory and the usual computation methods. We find remarkable agreement between observations and the Gibbs-Pitzer theory as implemented in FREZCHEM, both for brine salinity (RMSE=1.9 g/kg) and liquid H_2O mass fraction (RMSE=8.6 g/kg). On this basis, we propose expanded sea ice phase composition equations that include minerals, are expressed in terms of ITS-90 temperature and absolute salinity, and are valid down to the eutectic temperature ($-36.2°C$). These equations precisely reproduce FREZCHEM, outcompeting currently used calculation techniques. We also suggest a modification of the TEOS-10 seawater Gibbs function giving a liquidus curve consistent with observations down to the eutectic temperature without changing TEOS-10 inside its original validity range.

1 Introduction

Sea ice is composed of pure ice, liquid brine, hydrated salt minerals and gas bubbles (*Weeks and Ackley*, 1986; *Light et al.*, 2003; *Hunke et al.*, 2011). These multiple phases render sea ice structurally, thermodynamically, biologically and chemically different from freshwater ice (*Thomas*, 2017). Of all these constituents, brine is the most studied next to ice (see, e.g., *Notz*, 2005), and affects the ice thermal regime and seasonal cycle of ice thickness (e.g., *Untersteiner*, 1961; *Bitz and Lipscomb*, 1999; *Vancoppenolle et al.*, 2005; *Wiese et al.*, 2015) and, in turn, the seasonal evolution of ice extent and volume (*Semtner*, 1984; *Vancoppenolle et al.*, 2009; *Turner and Hunke*, 2015). The chemical composition and fraction of brine inclusions also largely determine the suitability of the sea ice biome for microbial life (*Arrigo and Sullivan*, 1992; *Thomas and Dieckmann*, 2002). Sea ice models represent brine inclusions from highly parameterized (*Semtner*, 1976) to more and more explicit approaches (e.g. *Bitz and Lipscomb*, 1999; *Griewank and Notz*, 2013;

Turner et al., 2013; *Moreau et al.*, 2015), whereas biogeochemical field-based sea ice studies often include brine inclusions as part of their characterization of the sea ice environment (*Miller et al.*, 2015).

Characterizing the sea ice phase composition is not trivial: phase composition changes with temperature T and salinity S, for two reasons. First, increasing salinity depresses the freezing temperature of seawater (*Doherty and Kester*, 1974) as fewer H_2O molecules are available to freeze (*Feistel*, 2008). Second, the crystalline lattice of solid H_2O hardly incorporates any salt because of size and charge constraints (*Weeks and Ackley*, 1986; *Petrich and Eicken*, 2009). Instead salt is dissolved in small (0.01-10 mm) liquid inclusions or hydrated into solid minerals (*Assur*, 1958; *Perovich and Gow*, 1996; *Marion et al.*, 1999; *Light et al.*, 2003). As the ice cools, brine inclusions adjust their freezing temperature to maintain equilibrium by shrinking, which increases their own salinity (S_{br}, also referred to as brine salinity) to values typically much larger than the bulk salinity of the ice (e.g., *Ono*, 1967). Meanwhile, more minerals precipitate and fewer liquid H_2O molecules remain, until exhaustion of all liquid at the *eutectic* point (T_e, S_e). The eutectic point indicates the salinity and temperature couple corresponding to the lowest possible seawater freezing temperature, below which all water becomes solid. The corresponding T-S values are referred to as *eutectic* temperature (T_e) and salinity (S_e). Both are constant for given pressure and composition.

The sequence of precipitating minerals under cooling has long been ambiguous. This is because the two main laboratory-based studies documenting the chemical evolution of brine from freezing down to eutectic temperatures (*Gitterman*, 1937; *Nelson and Thompson*, 1954) are not in exact agreement. Such differences are attributable to varying sample equilibration times: *Gitterman* used up to 4-week periods, whereas *Nelson and Thompson* used only a few hours (see *Marion et al.*, 1999, for thorough discussion). This in turn affects the mineral form into which calcium precipitates (gypsum or antarcticite) and ultimately changes T_e: $-36.2°C$ along the *Gitterman* pathway (gypsum) and $-54°C$ along the *Nelson & Thompson* pathway (antarcticite). The classical sea ice phase diagram (*Assur*, 1958; *Petrich and Eicken*, 2009), derived from algorithimic chemical computations, is directly based on *Nelson and Thompson's* data.

Ambiguities in the crystallization sequence, as well as variable calculation practices, undermine the confidence in calculated brine salinity S_{br} and mass (or volume) fraction

of brine ϕ, the most used descriptors of sea ice constitution. In observational studies (e.g., *Lannuzel et al.*, 2008; *Ewert and Deming*, 2013; *Miller et al.*, 2015), S_{br} and ϕ are typically computed from T and S measurements, using the observation-based empirical fits of *Cox and Weeks* (1983, 1986). Modelling authors (e.g., *Griewank and Notz*, 2013; *Turner et al.*, 2013; *Moreau et al.*, 2015) have used simpler, more consistent but less precise approaches: they specify brine salinity from T using a simple fit, either linear (*Bitz and Lipscomb*, 1999) or 3^{rd} order (*Notz and Worster*, 2009). Then brine fraction is retrieved as the ratio of bulk over brine salinity, which relies on the assumption that minerals are negligible. Brine fraction and salinity are fundamental to contemporary thermodynamic formulations in sea ice models, because they control all material thermodynamic properties (e.g., specific heat, thermal conductivity). It must be noted that all the aforementionned relationships derive from the algorithmic computations of *Assur* (1958). Willingly or not, these implicitly assume that the *Nelson and Thompson* (1954) crystallization pathway holds.

Two recent developments motivate us to revisit the sea ice phase composition problem. First, recent sea ice geochemical works (*Geilfus et al.*, 2013; *Butler and Kennedy*, 2015; *Butler et al.*, 2016a,b, 2017) studied the precipitation of minerals in sea ice and definitely state *Gitterman*'s mineral crystallization sequence as the reference equilibrium pathway. These experimental works are all excellently backed up by theoretical calculations based on Pitzer equations (*Pitzer*, 1991), implemented in the FREZCHEM code (*Marion et al.*, 1999). FREZCHEM predicts the temperature of precipitation of minerals and the composition of brine in good agreement with laboratory experiments (*Marion et al.*, 1999; *Butler et al.*, 2016a, 2017). The consistency of FREZCHEM with high-precision measurements of seawater freezing temperature (*Doherty and Kester*, 1974) within a few mK is also striking (*Feistel*, 2008).

The second development motivating us to reconsider the sea ice phase composition basis is the recent implementation into Earth System model components of standard thermodynamic descriptions of environmental fluids. Let us mention TEOS-10, the International Thermodynamic Equation of Seawater (*Feistel*, 2008; *IOC, SCOR and IAPSO*, 2010), which also includes expressions for ice *Ih* (*Feistel and Wagner*, 2006) and humid air (*IAPWS*, 2010). TEOS-10 is now included in some ocean models (*Roquet et al.*, 2015). These new thermodynamic equations are appealing in that they blend all thermodynamic properties of the considered material in a unique thermodynamic potential (such as a

Gibbs function), from which all other properties can uniquely and consistently be derived. Another advantage of such approaches as TEOS-10 is that they are based on clearly defined units. Celsius degrees, following the International Temperature Scale 1990, are the reference temperature units (ITS-90, *Preston-Thomas*, 1990), whereas g/kg are the reference units for absolute salinity (*Millero et al.*, 2008). The sea ice thermodynamic formulations currently used in Earth System models (see *Massonnet et al.*, 2012, Table 1) are based on physically well-founded approximations (typically from *Semtner*, 1976; *Bitz and Lipscomb*, 1999). However, in contrast with TEOS-10, these formulations were not built from a unique thermodynamic potential and therefore are somehow inconsistent. In addition, they are not clear in terms of which temperature and salinity units they use.

In light of these ideas, we revisit the sea ice phase composition subject, by confronting observations, theory (encapsulated in FREZCHEM) and frequently used computation methods. We focus on three main diagnostics: brine salinity, the mass fraction of salt that is hydrated into solid minerals, and liquid H_2O mass fraction. Our analysis suggests that FREZCHEM is currently the most consistent source on sea ice phase composition, and should therefore be used as a basis for revised sea ice phase composition. We also propose a revised set of sea ice phase equations accounting for solid minerals. Finally, we propose means to achieve compatibility with international standards, which requires modification of TEOS-10 below $-6°$C and above $S = 120$ g/kg. The updated sea ice phase equations and the TEOS-10 expansion provide a revised basis for sea ice thermodynamics. We first introduce the observational and theoretical materials used (Section 2), describe our results (Section 3) and discuss them (Section 4). The proposed modification of TEOS-10 is presented as an Appendix.

2 Theoretical framework and observational sources

A complete characterization of the sea-ice composition is given by the mass fractions of all of its constituents. Yet most applications need only a few diagnostics, in most cases, brine salinity and liquid fraction. In this section, we define the main sea ice phase composition diagnostics discussed in this paper, then review the observational and theoretical sources available to constrain them.

2.1 Diagnostics of sea ice phase composition

Our system is an isolated unit mass of H_2O and sea salt species with varying total mass but fixed relative proportions of the different salts, as given by the standard seawater composition (*Millero et al.*, 2008), at standard atmospheric pressure and thermodynamic equilibrium. The equilibrium assumption holds at time scales larger than a few minutes if only the ice-brine system is considered (*Griewank and Notz*, 2013). The equilibrium time scale can reach up to a few weeks if the slowest minerals such as gypsum are considered (*Marion et al.*, 1999). The system is either in the state of sea ice (if partly or entirely solid) or seawater (if entirely liquid). State variables are temperature T (ITS-90 °C, *Preston-Thomas*, 1990) and absolute bulk salinity S (g/kg, *Millero et al.*, 2008). The latter is defined as the absolute salinity of a well stirred, melted sea ice sample, of much larger size than individual brine inclusions. We seek to express phase composition diagnostics as functions of T and S.

Several extra assumptions are worth mentioning. Since we consider a unit mass as our fundamental system of interest (as done in FREZCHEM), most density-related issues can be discarded. In particular, we ignore gas bubbles as they have negligible mass. As phase relationships are derived in an isolated system framework, all heat and mass exchange (e.g. brine drainage) processes are ignored. Similarly, the textural type of sea ice (columnar or granular) is not considered. This is because textural types correspond to varying layouts of ice with the same *Ih* crystal structure, and therefore do not affect phase equilbrium. We also neglect pressure, the consequences of which are expectedly small but hard to evaluate in the present context of understanding.

At equilibrium, the chemical composition of brine (with regard to solutes) solely depends on T (*Feistel and Hagen*, 1998), hence brine salinity S_{br} is only function of T: brine inclusions are at their freezing point, which establishes a direct correspondence between both. This relation $S_{br}(T)$, called the *liquidus curve* is the reciprocal of the relation between the seawater freezing point and salinity, $T_f(S)$. That brine salinity solely depends on temperature at thermal equilibrium has long been assumed in thermodynamic sea ice formulations (e.g. *Ono*, 1967; *Worster*, 1992; *Bitz and Lipscomb*, 1999).

A well-behaved liquidus curve should verify two constraints. First, fresh ice should have 0°C as a freezing point, hence S_{br} should be nil on $T = 0$°C. Second, the liquidus curve should intersect the eutectic point. We set the eutectic temperature to $T_e = -36.2$°C,

following the theoretical arguments of *Marion et al.* (1999), and considering the *Gitterman* (1937) crystallization pathway as our reference. The eutectic salinity can hardly be determined experimentally: it corresponds to the salinity of brine with negligibly small volume, reached just above the eutectic temperature. Our choice for the eutectic salinity is to evaluate the third-order liquidus polynomial expression (regressed on selected observations and termed POLY3, see Section 2.3.1) on $T = T_e$, giving S_e=250.6146 g/kg.

The mass fraction of salt hydrated into minerals ϕ_{sm}^{salt} is proportional to the total mass of salt in the system, hence to S. As each mineral is in equilibrium with brine, and the composition of brine depends on T only, we postulate that ϕ_{sm}^{salt} follows:

$$\phi_{sm}^{salt} = f_{sm}(T) \cdot S, \tag{1}$$

where f_{sm}, the mass fraction of total salt complexed into minerals is only a function of T. For $f_{sm} = 0$, there are no minerals in the system. For $f_{sm} = 1$, all salts are stored into minerals, which must be the case below the eutectic temperature. In their study focused on mirabilite, *Butler et al.* (2016a, equation 6) make similar assumptions and reach a comparable but slightly different formulation of mirabilite mass fraction.

The mass fraction of brine (or liquid fraction ϕ_{br}) is another important diagnostic. Let us first write bulk salinity as the sum of brine and mineral contributions:

$$S = \phi_{br} \cdot S_{br}(T) + f_{sm}(T) \cdot S. \tag{2}$$

Rearranging terms, we get the liquid fraction:

$$\phi_{br}(S,T) = \left(1 - f_{sm}(T)\right) \cdot \frac{S}{S_{br}(T)}, \tag{3}$$

an expression close to that of *Assur* (1958). Classically used forms (e.g. *Bitz and Lipscomb*, 1999; *Notz and Worster*, 2009) ignore minerals. The liquid fraction simplifies into $\phi_{br} = S/S_{br}(T)$, which is reasonable as long as the mass fraction of minerals is negligibly small, but does not attain zero at T_e and below.

In some instances, rather than liquid fraction, one needs to retrieve the mass fraction of liquid H_2O, noted $\phi_{br}^{H_2O}$. The latter is brine fraction less the dissolved salt fraction (which for brine salinity in g/kg is $\phi_{br} S_{br} \cdot 10^{-3}$). Hence $\phi_{br}^{H_2O}$ directly relates to brine fraction:

$$\phi_{br}^{H_2O}(S,T) = \phi_{br}(S,T) \cdot \left(1 - S_{br}(T) \cdot 10^{-3}\right). \tag{4}$$

Using equation (4), one can derive liquid H_2O mass fraction from T and S through liquid mass fraction and salinity. An alternative expression directly relating $\phi_l^{H_2O}$ to f_{sm} and S_{br} can be obtained by substituting (3) into (4).

Another frequently used quantity is brine volume fraction (ϕ_{br}^v). Mass and volume fractions are similar but quantitatively different. Following a similar development for solid fractions (*Notz*, 2005, page 44) liquid mass and volume fractions can be converted into each other:

$$\phi_{br} = [1 + (1/\phi_{br}^v - 1)\rho_i/\rho_{br}]^{-1}, \tag{5}$$

$$\phi_{br}^v = [1 + (1/\phi_{br} - 1)\rho_{br}/\rho_i]^{-1}, \tag{6}$$

where ρ_i and ρ_{br} refer to pure ice and brine densities, for which following *Cox and Weeks* (1983), we used and the expressions of *Pounder* (1965) and *Zubov* (1945). In the upcoming sections, we will evaluate what theory and observations tell us about f_{sm}, S_{br} and ϕ_{br}.

2.2 Sea ice phase relationships from the Gibbs-Pitzer theory (FREZCHEM).

The Gibbs-Pitzer approach (*Pitzer*, 1991) implemented in the FREZCHEM code (*Marion et al.*, 2010), provides practical means to calculate the theoretical equilibrium composition of partly frozen electrolyte solutions – of which our system is a particular example. FREZCHEM is widely used to explore cold geochemical processes in the Earth's polar regions, and to explore life limits on Europa and Mars. Mass conservation at temperature T and salinity S, split over the different phases and integrated over the different chemical species considered by FREZCHEM is given by:

$$1 \quad = \quad \phi_{br}^{H_2O} + \phi_{br}^{salt} + \phi_{ice}^{H_2O} + \phi_{sm}^{H_2O} + \phi_{sm}^{salt}. \tag{7}$$

The different terms refer to mass fractions (ϕ's) of liquid H_2O, dissolved salts, pure ice (solid H_2O) and solid minerals split into H_2O and salt contributions, all being expressed per unit mass of sea ice. The phase diagram shown in Figure 1, drawn from post-processed FREZCHEM outputs with $S = 5$ g/kg (typical of first-year winter sea ice, taken for illustration) shows the distribution of mass among the different phases of the system, from the eutectic to the freezing temperature.

The principle of the Gibbs-Pitzer approach is to minimize the Gibbs free energy, in a form accounting for binary and ternary ion interactions, described through *Pitzer*

parameters fitted on experimental data. FREZCHEM includes tabulations of *Pitzer* parameters and a minimization algorithm for the Gibbs free energy. Based on a specified reference composition for an aqueous solution at a reference temperature, FREZCHEM gives the solute and mineral composition (activity coefficients and molal concentrations) at any temperature down to the eutectic limit. Because FREZCHEM is an equilibrium model, it is consistent with the *Gitterman* crystallization pathway (obtained from long equilibration times) with a eutectic temperature at -36.2°C (*Marion et al.*, 1999).

To derive the detailed Gibbs-Pitzer sea ice phase diagram, we used FREZCHEM 13.3, configured to simulate the cooling and progressive freezing of $M = 1000 + M_s$ grams of standard seawater, made of 1000 g of H_2O and $M_s = 1000 \cdot S/(1000 - S)$ grams of salt, adequately distributed among the 15 species of standard seawater (*Millero et al.*, 2008, Table 4). Following the composition of standard seawater, we also imposed 385 ppm of CO_2 and pH = 8.1. FREZCHEM was run 41 times for $S = 0.3, 1, 2, ..., 40$ g/kg. The cooling started from $T = 0°C$ down to the eutectic temperature over $-0.1°C$ steps. Minerals precipitated at temperatures independent of S (Table 1) and the simulated sequence nearly matches that found by *Butler et al.* (2016a). Differences in temperatures of precipitation are typically within 0.1°C and could be due to slightly different model version, input files or to numerical precision.

To derive mass fractions, the following FREZCHEM outputs were retained for post-processing: the mass of ice Ih (g), the mass of liquid H_2O (g), the molality of the 21 considered solutes (mol/kg liquid H_2O), and the moles of each of the considered 101 minerals (mol/kg), of which only 8 were found in detectable amounts (Table 1). All these outputs were stored over the 363×41 T-S grid for further processing. Throughout processing, we used the *Wieser* (2006) table of atomic weights to compute molar masses of indididual ions, solutes and minerals, as recommended by *Millero et al.* (2008).

Let us now describe how S_{br}, f_{sm}, ϕ_{br} and $\phi_{br}^{H_2O}$ were derived. For each solute, the mass fraction $C_i(S,T)$ (g/kg brine) was retrieved from molality. The FREZCHEM brine salinity value is the sum of the C_i's over all solutes:

$$S_{br}^{\mathrm{FZC}} = \sum_{\text{solutes}} C_i. \tag{8}$$

For each mineral, the mass fractions of solid salt $\phi_{sm,i}^{salt}$ (per unit mass of the system, g/kg) were derived as well. The salt fraction in minerals could be diagnosed as

$$f_{sm}^{\mathrm{FZC}} = \frac{1}{S} \cdot \sum_{\mathrm{minerals}} \phi_{sm,i}^{salt}. \tag{9}$$

A check indicated that the FREZCHEM C, S_{br} and f_{sm} values are as expected independent of S. The liquid H_2O fraction was diagnosed by dividing the mass of liquid H_2O by M. Brine mass fraction ϕ_{br} was finally retrieved from Equation 4.

To expand f_{sm}^{FZC} and S_{br}^{FZC} within the 363 discrete temperature values, we apply piecewise cubic hermite interpolation. To expand $\phi_{br}^{H_2O}$ we apply similar cubic interpolation in T and, because $\phi_{br}^{H_2O}$ is linear in S, we used linear interpolation in S.

2.3 Observational sources

Now we turn to the observational sources that constrain the sea ice phase composition. We strived to retain observational sources only. We focused on directly measured quantities in order to avoid inconsistencies due to processing.

2.3.1 Liquidus and freezing temperature

We retained four sources documenting either the liquidus salinity as a function of temperature or equivalently the freezing point of seawater versus salinity (*Gitterman*, 1937; *Nelson and Thompson*, 1954; *Doherty and Kester*, 1974; *Butler et al.*, 2016b, see Table 2, Figure 2). Unlike previous authors, we did not retain the model calculations of *Assur* (1958), as they were computational derivations of the *Nelson and Thompson* (1954) observations. All retained studies reported absolute salinities in g/kg. The conversion from ITP-68 to ITS-90 temperature scale was applied to the observations prior to 1990 (*Gitterman*, 1937; *Nelson and Thompson*, 1954; *Doherty and Kester*, 1974).

The experimental contexts in which these observations were acquired differ in a number of ways, in particular regarding the apparatus, instruments and type of seawater used, protocols and equilibration times. They therefore have varying T-S precision and range. We attempted to summarize these differences in Table 2, and discuss the most important points hereafter.

The experiments of *Gitterman* (1937) and *Nelson and Thompson* (1954) aimed to describe the sequence of precipitating salts from the freezing of seawater. To that pur-

pose, they followed the composition of the liquid phase in frozen artificial and natural seawater samples, respectively, at different temperatures. We used tabulated values provided in these two studies. *Gitterman* (1937) directly provides absolute salinity readings (their Table 7). *Nelson and Thompson* (1954) provide mass concentration for the most important ions ($Na^+, Mg^{2+}, Ca^{2+}, K^+, Cl^-, {SO_4}^{2-}$, their Table 1). To get absolute salinity, we summed these, excluding samples without ${SO_4}^{2-}$ reported value, which would under-estimate salinity by up to about 5-10%. Despite both studies being characterized by different incubation times (up to 4 weeks for *Gitterman* and a few hours for *Nelson and Thompson*) and crystallization pathways (*Marion et al.*, 1999), there is no clearly detectable liquidus salinity difference between both studies.

The observations of *Doherty and Kester* (1974) are high-precision measurements of the freezing point of seawater over the observed seawater salinity range. These data were indireclty used for the elaboration of TEOS-10 (see Section 6.3 of *Feistel*, 2008). They are provided in two tables in the original publication. We followed *Feistel* (2008) and corrected for the effect of air saturation and converted from IPTS-68 to ITS-90 temperature scales, even though such conversions appear negligible for our purposes.

Butler et al. (2016b) focussed on the precipitation of mirabilite in synthetic Simplified seawater samples (*DOE*, 1994) using close-bottle incubation methods and an average incubation time of 53 days, using the opportunity to note the freezing point of seawater, down to -20.6°C. Synthetic Simplified seawater only has the 6 major ions, in slightly higher proportions than in natural seawater, in order to compensate for the missing minor ions while preserving salinity.

In conformity with our assumption that the *Gitterman* (1937) crystallizationpathway holds, all of our analyses are restricted to the $[-36.2, 0$°C$]$ temperature range. Altogether, we retained 64 T-S couples covering the $[-35.49, -0.37$°C$]$ temperature and $[6.97, 248.4$ g/kg$]$ salinity ranges (symbols in Fig. 2). Between -20 and -10° C, where data coverage is the largest, we note a typical uncertainty of about 2.5 g/kg for S_{br}, which corresponds to a temperature uncertainty of ~ 0.15°C, that can be attributed to varying apparatus, incubation time and type of samples used.

A 3^{rd} order polynomial was fitted on the selected 64 observations under the constraint that $S_{br} = 0$ at $T = 0$:

$$S_{br}^{POLY3} = -18.7\ T - 0.519\ T^2 - 0.00535\ T^3. \tag{10}$$

This fit (black line in Fig. 2) referred to as POLY3 was used to provide the best observational estimate of the eutectic salinity $S_e = 250.6146$ g/kg.

2.3.2 Minerals

There are also a few observational sources that can help to construct the solid salt fraction function f_{sm}. Among the visual (e.g., *Light et al.*, 2009; *Geilfus et al.*, 2013), analytical (e.g., *Gitterman*, 1937; *Butler et al.*, 2016a) and X-ray methods (*Butler and Kennedy*, 2015) that have been applied, we retain analytical estimates of mirabilite mass per unit mass of sea ice by *Butler et al.* (2016a) using the fit they provide (their Table 4). For reference, we also converted the tabulated salt mass of minerals from the calculations of (*Assur*, 1958, Table 3) into f_{sm}.

2.3.3 Liquid H_2O fraction

Liquid fraction cannot be directly measured, but liquid H_2O can be retrieved by Nuclear Magnetic Resonance (NMR) (*Richardson and Keller*, 1966). The NMR signal, namely the area under the NMR absorption curve, is related to the liquid H_2O mass fraction in a sample. *Richardson and Keller* (1966) measured the NMR absorption curves from frozen seawater samples at 10.022 and 35.035 g/kg, from freezing temperatures down to -50°C. Since these experiments span a wide region of the T-S space and are well documented, they are suitable for an evaluation of liquid water fraction. Their table data included some unreproducible processing, hence we chose to digitize the raw NMR liquid H_2O mass fraction estimates presented in their Figure 2 and 3. We specifically use the ratio between NMR area at temperature T to NMR area at 0°C, where the sample is all liquid (termed Q_T/Q_0 in their paper). The authors mention that their results were reproducible within 1% accuracy, to which must be added the digitizing uncertainty.

2.4 The liquidus curve from a modified TEOS-10

Another source to be considered is the International Thermodynamic Equation Of Seawater, aka *TEOS-10* (*IOC, SCOR and IAPSO*, 2010), which provides means to consistently derive all seawater's thermodynamic properties, including the freezing point of seawater. The freezing point can be numerically inverted – resulting into a liquidus curve. TEOS-10 is now the international reference used in the framework of oceanographic anal-

yses. It is also implemented into some ocean models and thermodynamic sea ice formulations should ideally be consistent with TEOS-10.

The information on the seawater freezing point that was blended into the TEOS-10 seawater Gibbs function comes from FREZCHEM (*Feistel*, 2008), found to agree within a few mK with the observations of *Doherty and Kester* (1974). Operationally, the TEOS-10 freezing point derives from the freezing condition equation, stating the equality of the chemical potentials of ice and of water in seawater.

The first initial obstacle towards a TEOS-10 liquidus curve is that the TEOS-10 validity range is limited to $S < 120$ g/kg, which is insufficient to get a liquidus curve over the proper salinity range. One obvious initial attempt to resolve that issue is to relieve the 120 g/kg salinity barrier from the TEOS-10 computations, that is, continue to use the seawater Gibbs function of TEOS-10 outside its range of validity. The resulting freezing point (dashed blue curve in Figure 2) is not only imprecise as expected, it is also not monotonic, reaching a maximum of -22.3°C near $S = 330$ g/kg, hence the reciprocal function (the liquidus curve) can only be defined above -22.3°C.

The reference TEOS-10 is therefore inappropriate for the estimation of a proper liquidus curve. It is however possible to add a small modification to TEOS-10 to address this problem, which we detail in Appendix A and only summarize here. In this development, as explained by *Feistel and Hagen* (1998), brine is viewed as the continuation of seawater, being characterized by the same Gibbs function, expressed as a function of brine salinity. This approach is well posed: above the freezing point, brine fraction is 1 and bulk and brine salinity coincide.

Turning now to the desired correction to the TEOS-10 Gibbs potential, the basic idea is to introduce a perturbation $g^c(S)$ to the TEOS-10 seawater Gibbs potential $g^{TEOS-10}$:

$$g(S_{br}, T) = g^{TEOS-10}(S_{br}, T) + g^c(S_{br}). \tag{11}$$

g^c should be constructed so as to minimize changes in g within the TEOS-10 salinity range, and to fit the freezing temperature at higher salinities (see Fig. A2). The most convenient form we found for the perturbation function is:

$$g^c(S_{br}) = \begin{cases} 0 & \text{if } S_{br} < S_0 = 120 \text{ g/kg}, \\ a \cdot (S_{br} - S_0)^4 & \text{otherwise (where } a = 1.2370 \times 10^{-5} \text{ J/g}^4 \cdot \text{kg}^3), \end{cases} \tag{12}$$

which has the few desired properties. The liquidus curve derived from the modified Gibbs function (mTEOS-10, solid blue curve in Figure 2) is now reasonably precise down to T_e. It also preserves TEOS-10 integrity below $S_0 = 120$ g/kg and ensures the continuity of the Gibbs function's derivatives up to order 4. Finally, it is eutectic compliant by definition. The method outlined above and developed in the appendix is efficient to derive a proper liquidus curve from the seawater Gibbs function. However, there could be extra deviations to the Gibbs function off the freezing curve that cannot be inferred from our method.

3 Results

In this section, we describe how the Gibbs-Pitzer theory (FREZCHEM), observations and classical computation methods compare in terms of liquidus curve, salt fraction in minerals and liquid fraction.

3.1 Liquidus curve

The liquidus curves from the various retained sources are presented graphically, versus temperature (Figure 2). The computation methods (empirical functions, TEOS-10) that were used are listed in Table 3. For quantitative comparison, the 64 retained observed temperatures of Section 2.3 were used as a basis for the liquidus salinity computation. The mean statistics of the comparison between the calculated salinities with observed values are given in Table 4.

All sources give the increase in brine salinity with decreasing temperature, and most of them predict a monotonic increase from 0 to ~ 250 g/kg with an initially rapid increase near the freezing temperature, then slowing down approaching T_e.

The FREZCHEM liquidus provides the best match with observational values, giving a slightly positive bias (1.1 g/kg), a root-mean-square (RMSE) error of 1.9 g/kg and a standard deviation of error (STDE) of 2.5 g/kg, characterizing the current levels of uncertainty on the liquidus salinity. Uncertainties increase with decreasing temperature: for instance, the FREZCHEM-obs RMSE is more than three times smaller over the TEOS-10 validity range (RMSE= 0.5 g/kg, STDE = 1.15 g/kg) than over the entire temperature range. Near-freezing temperatures are also where we have the most precise observations (*Doherty and Kester*, 1974, hereafter DK74), as illustrated by the error versus

temperature plot (Fig. 2b). The precision of the DK74 observations clearly outcompetes the other observations, among which the observations of *Butler et al.* (2016b) seem the least biased compared to FREZCHEM.

FREZCHEM relies on a precise and coherent representation of thermo-chemical processes, which explains why it is able to capture the inflection in brine salinity at $-22.9°C$ associated with the precipitation of hydrohalite. This constitutes a clear advantage of FREZCHEM over other approaches. For instance, the observation-based 3^{rd} order least-square fit (POLY3, black line in Fig. 2) cannot capture the liquidus inflection and does not reproduce observations as well as FREZCHEM (RMSE=2.3 g/kg, STDE = 3.2 g/kg).

Several other classically used approaches for estimation of the liquidus curve were also included in our evaluation (see Table 3). The simplest possible approach is to assume that the relation between T and S_{br} is linear (*Assur*, 1958). Such a relation would hold if brine was an ideal solution, i.e., if the different molecules that compose brine interacted all in the same way. This is seemingly valid until about $-5°C$, below which non-linearities become significant (see red dotted line in Fig. 2), leading to largely over-estimated brine salinities (> 100 g/kg) at low temperatures. The linear approach is used in the many sea ice models following the *Bitz and Lipscomb* (1999) thermodynamic formulation, based on the plausibly negligible impact of brine salinity errors on the energetics of the system (*Notz*, 2005).

Biogeochemical sea ice modules are sensitive to the large brine salinity bias at low temperature in the linear approach, notably for primary production (*Vancoppenolle and Tedesco*, 2017) and carbonate chemistry computations (*Moreau et al.*, 2015), calling for better brine salinity estimates. As an example of the many 3^{rd} order fits available, we retained the third-order polynomial of *Notz and Worster* (2009, NW09 in Table 3), fitted on the liquidus reconstruction of *Assur* (1958) over the $[-22.9, 0°C]$ range. The NW09 fit fullfills the fresh ice constraint, but not the eutectic constraint and expectedly spreads from observations below the hydrohalite precipitation point (solid red line in Fig. 2).

The last empirical approach included in our evaluation is the *Cox and Weeks* (1986, their Table 2) relationship (gray line in Fig. 2, CW86 in Table 3), widely used in the observational literature. CW86 combines three 3^{rd} order polynomials regressed on *Assur* (1958) data and holds from -2 to $-54°C$ (the eutectic temperature under the *Nelson and Thompson* crystallization pathway). Because it does not cover the high tempera-

ture range, the CW86 approach is unsuitable for modelling. Yet the CW86 function still provides precise liquidus estimates (RMSE = 2.9 g/kg, STDE= 3.5 g/kg), including the −22.9°C discontinuity, among the most precise estimates retained.

The modified TEOS-10 (mTEOS-10) liquidus is in line with the best available estimates. It is slightly less precise on average than other approaches (RMSE = 3.0 g/kg, STDE = 4.6 g/kg). It is remarkable that mTEOS-10 is the most precise estimation approach over the TEOS-10 validity range, nearly as precise as FREZCHEM (RMSE = 0.6 g/kg, STDE = 1.14 g/kg). In the [−10, −20°C] range, mTEOS-10 overestimates the liquidus salinity by about 5 g/kg and significantly underestimates it near the hydrohalite precipitation discontinuity (Fig 2e).

3.2 Minerals

Experimental sources for estimating the salt fraction in minerals f_{sm} are only a few (see Section 2.3). Figure 3 graphically depicts $f_{sm}(T)$ from FREZCHEM (grey line), the *Assur* (1958) computations (red dashed line), and the observation-derived fit of *Butler et al.* (2016a, hereafter B16a, blue squares), which only includes mirabilite and hence is valid until −22.9°C. Because mirabilite dominates by far the total mass of minerals above that temperature threshold, the B16b fit is in excellent agreement with FREZCHEM, which itself includes all minerals.

At −22.9°C, the fraction of salt in minerals consistently reaches about 10% according to all sources. Below −22.9°C, the only independent source available is *Assur* (1958). We find agreement with FREZCHEM within 10% until about −33°C, where f_{sm} becomes slightly less than 0.8, because both approaches converge on the precipitation of hydrohalite. We do not expect the solution of Pitzer equations given by FREZCHEM and the calculations of *Assur* to be exactly consistent, because of the many differences between them.

The last two jumps in f_{sm} predicted by FREZCHEM are mostly due to the precipitation of meridianite and sylvite near −33.3°C and to magnesium chloride dodecahydrate at −36.2°C (Table 1). The FREZCHEM crystallization sequence we get is close to but slightly different from similar FREZCHEM computations (*Marion et al.*, 1999; *Butler et al.*, 2016a). It is beyond the scope of this work to track down the origin of the

differences, but they are presumably due to protocol differences (FREZCHEM version, specification of the input seawater composition).

3.3 Liquid H_2O fraction

Liquid mass (ϕ_{br}) or volume (ϕ_{br}^{v}) fractions are frequently used in sea ice studies, but not directly observable. However what can be learned from liquid H_2O fraction ($\phi_{br}^{H_2O}$), measurable by NMR, is in practice relevant to ϕ_{br} and ϕ_{br}^{v}. Indeed, these three quantities are closely related to each other. This is illustrated in the two scatter plots of Figure 4, based on the FREZCHEM diagnostics over the entire T-S space. First, both $\phi_{br}^{H_2O}$ and ϕ_{br}^{v} are tightly linearly correlated with ϕ_{br} – the associated linear regression coefficient is in both cases slightly smaller than 1. Second, the relation between $\phi_{br}^{H_2O}$, ϕ_{br}^{v} and ϕ_{br} is strictly monotonic. $\phi_{br}^{H_2O}$ and ϕ_{br}^{v} prove systematically lower than liquid mass fraction, with differences typically within 20 %. For liquid H_2O this is simply because next to H_2O brine also contains dissolved salt. For brine volume fraction this is due to the higher density of brine than that of the surrounding ice. Since ϕ_{br} and ϕ_{br}^{v} are nearly equivalent to $\phi_{br}^{H_2O}$, the coming paragraphs are nearly entirely focused on the latter.

The liquid H_2O fractions from the various retained sources are presented graphically, in an attempt to reproduce the two *Richardson and Keller* (1966) series of NMR scans, run at two different salinities (10.022 and 35.035 g/kg) over the [−35, 0°C] temperature range (Figure 5). For a quantitative evaluation of T- and S-based computations of the liquid water fraction, the observed T and S were used to estimate the observed liquid water fraction, for several variants in the details of the computations. In all cases but two, calculations were based on equations (3) and (4), which require intermediate calculations of liquidus salinity and solid salt fraction, for which several choices were tested. The mean statistics of the comparison with the 20 retained observational data points (Section 2.3.3) are given in Table 5.

All observational and theoretical sources suggest a decrease in $\phi_{br}^{H_2O}$, from nearly $1 - S \times 10^{-3}$ at the freezing temperature to nearly 0 at the eutectic temperature, and all sources obviously capture the increase in $\phi_{br}^{H_2O}$ with bulk salinity. Both FREZCHEM and observations feature discontinuities. Observations indicate a single discontinuity at −22.9°C, the temperature of hydrohalite precipitation. There are three discontinuities in FREZCHEM, each of them being associated with the precipitation of a mineral. The

absence of the last two discontinuities from observations is not surprising as (i) these are characteristic of the *Gitterman* equilibrium crystallization pathway simulated by FREZCHEM and (ii) the equilibration time is not mentionned in their study, it is unlikely that the required weeks for equilibration of samples (*Marion et al.*, 1999) were actually respected by *Richardson and Keller* (1966).

FREZCHEM (grey circles in Fig 5) provides the most consistent $\phi_{br}^{\mathrm{H_2O}}$ estimate with observationsand is slightly biased (1.1 g/kg, RMSE = 8.6 g/kg, STDE =13.3 g/kg), quantifying the current uncertainty levels on the liquid H_2O fraction. Uncertainties seem independent of temperature, but they increase from a RMSE = 2.9 g/kg for $S = 10.022$ g/kg, to 10.1 g/kg for $S = 35.035$ g/kg – provided we rule out the one sample processed at the highest temperature (see Fig. 5b).

Let us now discuss the few other simpler calculation techniques for liquid water fraction. Computations stem from equations (3) and (4) with prescribed functional dependencies for $S_{br}(T)$ and $f_{sm}(T)$. Using interpolated FREZCHEM values for S_{br} and f_{sm} gives virtually the same $\phi_{br}^{\mathrm{H_2O}}$ error statistics as for the direct FREZCHEM diagnostic, which confirms the internal consistency of the equations. The small difference is likely due to numerical precision or interpolation errors. Keeping the FREZCHEM values for f_{sm} but now using the slightly less precise liquidus estimates (mTEOS-10, blue curve in Fig. 5; POLY3, not shown but similar) instead of the FREZCHEM function only slightly deteriorates the liquid water error statistics (RMSE = 8.9 g/kg, STDE = 13.5 g/kg).

Accounting for minerals is necessary to reproduce the discontinuities in liquid content. Once f_{sm} is set to zero (i.e., once minerals are neglected, as classically done in sea ice models) the hydrohalite discontinuity at $-22.9°$C is lost, and errors in liquid H_2O fraction increase toward lower temperatures. With no minerals and a non-linear liquidus (black curve in Fig. 5), $\phi_{br}^{\mathrm{H_2O}}$ is overestimated, in particular below the hydrohalite discontinuity. With no minerals and linear liquidus (red dashed curve in Fig. 5), $\phi_{br}^{\mathrm{H_2O}}$ is underestimated for most of the temperature range.

The widely used empirical formulation for brine volume fraction of *Cox and Weeks* (1983, hereafter CW83) – a non-linear, piece-wise combination of 3^{rd} order functions – was also included in the analysis. The CW83 volume fraction was first converted into mass fraction from equation (5), using the CW83 expressions suggested for ice and brine densities. Then the result was combined with the liquidus salinity of *Cox and Weeks* (1986)

and converted into liquid H_2O fraction using equation (4), see Table 5. The result is slightly less consistent with observations than FREZCHEM (RMSE = 10.5 g/kg, STDE = 12.4 g/kg) over its claimed validity range ([−30, −2°C]).

We now finally turn to brine mass fraction estimates, taking FREZCHEM as a reference in the absence of observational values (Figure 6, Table S1). All findings on $\phi_{br}^{H_2O}$ practically apply to ϕ_{br}. The differences in calculated brine fraction and FREZCHEM values over the entire T-S space generalize Figure 5. With minerals included, FREZCHEM and mTEOS-10 agree within 3 g/kg in terms of brine fraction. Neglecting minerals induces the largest brine fraction errors, of up to about 20-30 g/kg in the low temperature range. Uncertainties at typical T-S values are generally low.

4 Discussion and conclusions

We revisited the thermodynamics of sea ice phase composition by confronting observations, theory and classical computation methods, from a revised formulation of the problem and a thorough account for available sources of information. We focused on two important diagnostics: brine salinity and liquid H_2O fraction (a close proxy of brine mass or volume fraction). All materials presented here are based on ITS-90 Celsius temperatures (*Preston-Thomas*, 1990) and absolute salinities in g/kg (*Millero et al.*, 2008), which is a prerequisite for compatibility with TEOS-10.

Observations of brine salinity and liquid H_2O fraction were carefully selected from a literature survey. As a theoretical reference, we used a detailed description of sea ice phase composition derived from FREZCHEM, a numerical code applying the Gibbs-Pitzer theory to aqueous solutions and widely used in Earth and Planetary science (*Marion et al.*, 2010). The considered T-S range encompasses virtually all sea ice conditions encountered on Earth: bulk salinity ranges over [0.3, 40 g/kg] and temperature goes from eutectic to liquid seawater conditions $[-36.2, 0°C]$. Standard seawater composition (*Millero et al.*, 2008) was strictly imposed at 0°C. Brine salinity, liquid H_2O fraction and brine mass fraction were derived based on FREZCHEM outputs, among other phase composition diagnostics.

The agreement between observations and the Gibbs-Pitzer theory (FREZCHEM) is remarkable: among all tested methods, FREZCHEM is the most faithful to observations, both in terms of brine salinity and liquid H_2O mass fraction. The agreement is

552 impressive given how independent FREZCHEM and the selected observations are, rais-
553 ing confidence in both. The resulting view of the sea ice phase composition does not sig-
554 nificantly depart from the standard one (*Assur*, 1958; *Petrich and Eicken*, 2009): sea
555 ice is typically ice and brine above $-22.9°C$ with a small fraction of mirabilite, taking
556 up to 10% of the salt mass. Most mineral precipitation occurs in the form of hydrohalite
557 between $-22.9°C$ and the eutectic temperature ($-36.2°C$) (Figure 1). The most notable
558 change in the revised phase diagram is a different succession of precipitating minerals,
559 and a eutectic temperature at $-36.2°C$ and not $-54°C$, consistently with the long equi-
560 libration times in the *Gitterman* crystallization pathway.

561 Uncertainties in sea ice phase composition are now better understood and quan-
562 tified. First, the typical error (RMSE) in brine salinity is 1.9 g/kg, larger near the hy-
563 drohalite precipitation temperature and smallest near the freezing point. Second, the mean
564 uncertainty in liquid mass fraction of H_2O, was evaluated at 8.6 g/kg (corresponding to
565 0.8% in the usual units, namely % of mass). Errors in brine mass or volume fractions
566 should have similar magnitude. Below $-22.9°C$, we find generally larger uncertainties
567 in liquid fraction, because of unresolved ambiguities in the mineral precipitation sequence.

568 Among all the assumptions made, neglecting pressure has the least known conse-
569 quences. Ignoring pressure effects on the freezing point is reasonable at the ocean sur-
570 face. Pressure effects might be comparatively larger within brine inclusions, and this topic
571 just starts being studied. Calculations based on isolated brine pocket volume changes
572 (*Crabeck et al.*, 2019) suggest typical pressures of 10 bars, and values up to 75 bars. To
573 envision possible implications on sea ice phase composition, we ran FREZCHEM at $p =$
574 100 bars. Even at such pressures, changes in brine salinity and in the predicted sequence
575 of precipitating minerals, relative to runs at 1 bar, were minor. Another instance of pos-
576 sibly significant pressure-related effects is marine ice, formed under marine ice shelves
577 from the freezing of seawater, several hundreds of meters deep into seawater, where the
578 seawater freezing point is a few tenths of K lower than at the surface. Admittedly, in Earth
579 System Models, the absence of pressure as a state variable in our proposed sea ice phase
580 relationships could be a source of inconsistency between the ice and seawater thermo-
581 dynamic formulations, at depth, and provided that marine ice is treated as sea ice. How-
582 ever, current understanding suggests that marine ice often proves nearly fresh (*Eicken*
583 *et al.*, 1994). More generally, how marine ice thermodynamics should be represented in
584 models is open to question.

There are also ambiguities in the sequence of crystallizing minerals that remain unresolved. This is notably because all formulations to date assume thermal equilibrium. In natural sea ice, temperature can change over a few hours, whereas the kinetics of mirabilite dissolution and gypsum precipitation are slower, slow enough to require sample equilibration times of up to a few weeks in the *Gitterman* equilibrium crystallization pathway (*Marion et al.*, 1999).

Another source of uncertainty is deviation from standard seawater composition. Compositional differences due to source seawater composition are expectedly minor (*McDougall et al.*, 2012). Mineral precipitation, could also change the composition of brine with respect to seawater. Hence brine convection (*Wells et al.*, 2011) exchanging brine and seawater could to some extent modify the sea ice composition. Yet, as brine convection and mineral precipitation are most efficient at fairly different depths in the ice, the former near the ice base, the latter near the ice surface, such deviations in brine composition seem unlikely to play a large role. By all means, to resolve these issues, one should relieve the phase equilibrium hypothesis and include the kinetics of mineral precipitation, which would bring the model's complexity to a much higher level. Since errors in brine composition remain relatively low (*Marion et al.*, 1999), we argue that these uncertainties are of minor importance as far as a salt budget is concerned and that there is no urgent need for such modifications.

We now turn to a few recommendations on working practises for calculating brine salinity and mass fraction in the context of observational measurements. Depending on the precision required, different computation approaches to the sea ice phase composition diagnostics can be adopted. The most precise and consistent source available for such computations is FREZCHEM. Since running it can take time, we provide the numerical FREZCHEM full phase composition description in netcdf format as supplementary material, which can readily be used. The classical fits of *Cox and Weeks* (1983, 1986) are very good but slightly less precise approximations, and are more limited in coverage. For temperatures above $-22.9°C$, using the POLY3 fit (eq. 10) to compute brine salinity and neglecting minerals to compute brine fraction is simple and precise enough for most purposes. The modified TEOS-10 Gibbs function – keeping TEOS-10 unchanged over its validity range and giving a liquidus curve in much better agreement with observations down to the eutectic temperature – is most useful for modelling purposes.

The revised framework proposed in Section 2 could make sea ice models more precise with respect to phase composition, improve their physical robustness, notably by considering the presence of minerals, and bring possible consistency with TEOS-10. Yet doing so would require in-depth modifications of the thermodynamic core of existing models and increase their complexity. Whether that would be worth systematic implementation requires investigation. It already seems clear that since sea ice process models including biogeochemistry are quite sensitive to brine salinity errors (*Moreau et al.*, 2015; *Vancoppenolle and Tedesco*, 2017) they would benefit from using at least the POLY3 fit presented here. Coupled ice-ocean models would also gain from TEOS-10 consistency within ocean and sea ice components. Major impacts on large-scale sea ice dynamics are not expected, but the additional physical realism and consistency would reduce uncertainties in the simulated thermodynamics.

Acknowledgments

We gratefully thank Benjamin Butler for sharing liquidus salinity observations, Odile Crabeck for scientific discussions, two anonymous reviewers and Rainer Feistel for their detailed and constructive comments, and Ioulia Nikolskaia for help on some of the figures. This work was carried out under the auspices of BEPSII (Biogeochemical Exchange Processes at the Sea-Ice Interfaces), a network supported by the Scientific Committee on Antarctic Research (SCAR), the Climate and Cryosphere (CliC) project of the World Climate Research Programme (WCRP) and by the Surface Ocean Lower Atmosphere Study (SOLAS). MT acknowledges funding from the European Unions Horizon 2020 research and innovation programme through the EUROCHAMP-2020 Infrastructure Activity under grant agreement No 730997. T. McD. gratefully acknowledges Australian Research Council support through grant FL150100090.

641 ## References

642 Arrigo, K., and C. W. Sullivan (1992), The influence of salinity and temperature co-
643 variation on the photophysiological characteristics of antarctic sea ice microalgae,
644 *Journal of Phycology*, *28*, 746–756.

645 Assur, A. (1958), Composition of sea ice and its tensile strength, *A. Nat. Acad.*
646 *Sci./Nat. Res. Council, Arctic Sea Ice*, *598*, 106–138.

647 Bitz, C. M., and W. H. Lipscomb (1999), An energy-conserving thermodynamic
648 model of sea ice, *Journal of Geophysical Research*, *104*, 15,669–15,677.

649 Butler, B., and H. Kennedy (2015), An investigation of mineral dynamics in frozen
650 seawater brines by direct measurement with synchrotron X-ray powder diffraction,
651 *Journal of Geophysical Research*, *120*, 5686–5697, doi:10.1002/2015JC011032.

652 Butler, B., S. Papadimitriou, A. Santoro, and H. Kennedy (2016a), Mirabilite solu-
653 bility in equilibrium sea ice brines, *Geochimica et Cosmochimica Acta*, *182*, 40–54,
654 doi:10.1016/j.gca.2016.03.008.

655 Butler, B., S. Papadimitriou, and H. Kennedy (2016b), The effect of mirabilite
656 precipitation on the absolute and practical salinities of sea ice brines, *Marine*
657 *Chemistry*, *184*, 21– 31, doi:10.1016/j.marchem.2016.06.003.

658 Butler, B., S. Papadimitriou, S. Day, and H. Kennedy (2017), Gypsum and hydro-
659 halite dynamics in sea ice brines, *Geochim. Cosmochim. Acta*, *213*, 17–34.

660 Cox, G. F. N., and W. F. Weeks (1983), Equations for determining the gas and
661 brine volumes in sea-ice samples, *Journal of Glaciology*, *102*, 306–316.

662 Cox, G. F. N., and W. F. Weeks (1986), Changes in the salinity and porosity of
663 sea-ice samples during shipping and storage, *Journal of Glaciology*, *32*, 371–375.

664 Crabeck, O., R. Galley, L. Mercury, B. Delille, J.-L. Tison, and S. Rysgaard (2019),
665 Evidence of freezing pressure in sea ice discrete brine inclusions and its impact on
666 aqueous-gaseous equilibrium, *Journal of Geophysical Research (in revision)*.

667 DOE (1994), *Handbook of methods for the analysis of the various parameters of the*
668 *carbon dioxide system in sea water; version 2*, ORNL/CDIAC-74.

669 Doherty, B. T., and D. Kester (1974), Freezing point of seawater, *Journal of Marine*
670 *Research*, *32*, 285–300.

671 Eicken, H., H. Oerter, H. Miller, W. Graf, and J. Kipfstuhl (1994), Textural charac-
672 teristics and impurity content of meteoric and marine ice in the Ronne Ice Shelf,

673 Antarctica, *Journal of Glaciology*, *40*, 386–398.

674 Ewert, M., and J. Deming (2013), Sea ice microorganisms: Environmental
675 constraints and extracellular responses, *Biology*, *2*, 603–628, doi:10.3390/
676 biology2020603.

677 Feistel, R. (2008), A Gibbs function for seawater thermodynamics for −6 to 80°C
678 and salinity up to 120 g kg^{-1}, *Deep Sea Research (I)*, *55*, 1639–1671.

679 Feistel, R., and E. Hagen (1998), A Gibbs thermodynamic potential of sea ice, *Cold*
680 *Regions Science and Technology*, *28*, 83–142.

681 Feistel, R., and W. Wagner (2006), A New Equation of State for H_2O Ice Ih, *J.*
682 *Phys. Chem. Ref. Data*, *35*, 1021–1047.

683 Geilfus, N.-X., R. J. Galley, M. Cooper, N. Halden, A. Hare, F. Wang, D. H.
684 Søgaard, and S. Rysgaard (2013), Gypsum crystals observed in experimen-
685 tal and natural sea ice, *Geophysical Research Letters*, *40*(24), 6362–6367, doi:
686 10.1002/2013GL058479.

687 Gitterman, K. (1937), Thermitcheskii analis morskoi vody (Thermal analysis of sea
688 water), *Tech. rep.*, Trudy Solyanoy Laboratorii (SSSR), translation from 1971,
689 USA Cold Regions Research and Engineering Laboratory, Hanover, NH. CRREL-
690 TL-287.

691 Griewank, P., and D. Notz (2013), Insights into brine dynamics and sea-ice desalina-
692 tion from a 1d model study of gravity drainage, *J. Geophys. Res.*, *118*, 3370–3386,
693 doi:10.1002/jgrc.20247.

694 Hunke, E. C., D. K. Notz, A. Turner, and M. Vancoppenolle (2011), The multi-
695 phase physics of sea ice: a review for modellers, *The Cryosphere*, *5*, 989–1009.

696 IAPWS (2010), Guideline on an equation of state for humid air in contact with
697 seawater and ice, consistent with the IAPWS formulation 2008 for the thermo-
698 dynamic properties of seawater, *Tech. rep.*, International Association for the
699 Properties of Water and Steam, Niagara Falls, Canada.

700 IOC, SCOR and IAPSO (2010), *The international thermodynamic equation of sea-*
701 *water - 2010: Calculation and use of thermodynamic properties*, Intergovernmental
702 Oceanographic Commission, Manuals and Guides No. 56, UNESCO (English).

703 Lannuzel, D., V. Schoemann, J. de Jong, L. Chou, B. Delille, S. Becquevort, and
704 J.-L. Tison (2008), Iron study during a time series in the western Weddell pack
705 ice, *Marine Chemistry*, *108*, 85–95, doi:10.1016/j.marchem.2007.10.006.

706 Light, B., G. A. Maykut, and T. C. Grenfell (2003), Effects of temperature on the
707 microstructure of first-year Arctic sea ice, *Journal of Geophysical Research*, *108*,
708 3051, doi:10.1029/2001JC000887.

709 Light, B., R. E. Brandt, and S. G. Warren (2009), Hydrohalite in cold sea ice: Lab-
710 oratory observations of single crystals, surface accumulations, and migration rates
711 under a temperature gradient, with application to "Snowball Earth", *Journal of*
712 *Geophysical Research*, *114*, C07,018, doi:10.1029/2008JC005211.

713 Madec, G., and the NEMO team (2008), NEMO ocean engine, *Note du Pôle de*
714 *modélisation 27 ISSN 1288–1619*, Institut Pierre-Simon Laplace (IPSL), France.

715 Marion, G., R. Farren, and A. J. Komrowski (1999), Alternative pathways for
716 seawater freezing, *Cold Regions Science and Technology*, *29*(3), 259 – 266, doi:
717 10.1016/S0165-232X(99)00033-6.

718 Marion, G., M. Mironenko, and M. Roberts (2010), FREZCHEM: A geochemical
719 model for cold aqueous solutions, *Computers and Geosciences*, *36*, 10–15.

720 Massonnet, F., T. Fichefet, H. Goosse, C. M. Bitz, G. Philippon-Berthier, M. M.
721 Holland, and P.-Y. Barriat (2012), Constraining projections of summer arctic sea
722 ice, *The Cryosphere*, *6*, 1383–1394.

723 McDougall, T. J., D. R. Jackett, F. J. Millero, R. Pawlowicz, and P. M. Barker
724 (2012), A global algorithm for estimating absolute salinity, *Ocean Science*, *8*,
725 1123–1134.

726 Miller, L. A., F. Fripiat, B. T. T. Else, J. Bowman, K. A. Brown, R. E. Collins,
727 M. Ewert, A. Fransson, M. Gosselin, D. Lannuzel, K. M. Meiners, C. Michel,
728 J. Nishiokan, D. Nomuar, S. Papadimitriou, L. M. Russell, L. L. Sorensen,
729 D. N. Thmas, J.-L. Tison, M. A. van Leeuwe, M. Vancoppenolle, E. W. Wolff,
730 and J. Zhou (2015), Methods for Biogeochemical Studies of Sea Ice: The
731 State of the Art, Caveats, and Recommendations, *Elementa*, *3*, 000,038, doi:
732 10.12952/journal.elementa.000038.

733 Millero, F. J., R. Feistel, D. G. Wright, and T. J. McDougall (2008), The composi-
734 tion of standard seawater and the definition of the reference-composition salinity
735 scale, *Deep-Sea Research I*, *55*, 50–72.

736 Moreau, S., M. Vancoppenolle, B. Delille, J.-L. Tison, J. Zhou, M. Kotovitch,
737 D. N. Thomas, N.-X. Geilfus, and H. Goosse (2015), Drivers of inorganic car-
738 bon dynamics in first-year sea ice: A model study, *J. Geophys. Res.*, *120*, doi:

10.1002/2014JC010388.

Nelson, K., and T. Thompson (1954), Deposition of salts from sea water by frigid concentration, *J. Mar. Res*, *13*, 166–182.

Notz, D. (2005), Thermodynamic and fluid-dynamical processes in sea ice, Ph.D. thesis, University of Cambridge.

Notz, D., and M. G. Worster (2009), Desalination processes of sea ice revisited, *Journal of Geophysical Research*, *114*, C05006, doi:10.1029/2008JC004885.

Ono, N. (1967), *Physics of snow and ice: proceedings of the International Conference on Low Temperature Science. I. Conference on Physics of Snow and Ice, II. Conference on Cryobiology. (August, 14-19, 1966, Sapporo, Japan)*, chap. Specific heat and heat of fusion of sea ice, pp. 599–610, Institute of Low Temperature Science, Hokkaido, Japan.

Perovich, D. K., and A. J. Gow (1996), A quantitative description of sea ice inclusions, *Jounal of Geophysical Research*, *101*, 18,327–18,343.

Petrich, C., and H. Eicken (2009), *Sea ice (2nd edition)*, chap. Growth, structure and properties of sea ice, pp. 23–77, Wiley-Blackwell.

Pitzer, K. S. (1991), *Activity coefficients in electrolyte solutions (Second Edition)*, CRC Press.

Pounder, E. R. (1965), *The Physics of Ice*, Pergamon Press, Oxford, UK.

Preston-Thomas, H. (1990), The international temperature scale of 1990 (its-90), *Metrologia*, *27*, 3–10.

Richardson, C., and E. E. Keller (1966), The brine content of sea ice measured with a nuclear magnetic resonance spectrometer, *Journal of Glaciology*, *6*, 89–100.

Roquet, F., G. Madec, T. J. McDougall, and P. M. Barker (2015), Accurate polynomial expressions for the density and specific volume of seawater using the TEOS-10 standard, *Ocean Modelling*, *90*, 29–43.

Semtner, A. J. (1976), A model for the thermodynamic growth of sea ice in numerical investigations of climate, *Journal of Physical Oceanography*, *6*, 379–389.

Semtner, A. J. (1984), On modelling the seasonal thermodynamic cycle of sea ice in studies of climatic change, *Climatic Change*, *1*, 27–37.

Thomas, D. N. (Ed.) (2017), *Sea ice (3^{rd} edition)*, Wiley-Blackwell.

Thomas, D. N., and G. S. Dieckmann (2002), Antarctic sea ice - a habitat for extremophiles, *Science*, *295*, 641–644.

Turner, A. K., and E. C. Hunke (2015), Impacts of a mushy-layer thermodynamic approach in global sea-ice simulations using the cice sea ice model, *J. Geophys. Res. Oceans*, *120*, 1253–1275.

Turner, A. K., E. C. Hunke, and C. M. Bitz (2013), Two modes of sea-ice gravity drainage: A parameterization for large-scale modeling, *J. Geophys. Res. Oceans*, *118*, doi:10.1002/jgrc.20171.

Untersteiner, N. (1961), On the Mass and Heat budget of Arctic Sea Ice, *Arch. Meteorol. Geoph. Bioklimatol. Ser. A*, *12*, 151–182.

Vancoppenolle, M., and L. Tedesco (2017), *Sea Ice, 3rd edition*, chap. Numerical models of sea ice biogeochemistry, p. 664, ISBN: 978-1-118-77838-8, Wiley-Blackwell.

Vancoppenolle, M., T. Fichefet, and C. M. Bitz (2005), On the sensitivity of undeformed Arctic sea ice to its vertical salinity profile, *Geophysical Research Letters*, *32*, L16502, doi:10.1029/2005GL023427.

Vancoppenolle, M., T. Fichefet, and H. Goosse (2009), Simulating the mass balance and salinity of Arctic and Antarctic sea ice. 2. Sensitivity to salinity processes, *Ocean Modelling*, *27 (1–2)*, 54–69, doi:10.1016/j.ocemod.2008.11.003.

Weeks, W. F., and S. F. Ackley (1986), *The Geophysics of sea ice*, *NATO ASI Series. Series B, Physics*, vol. 146, chap. The growth, structure, and properties of sea ice, pp. 9–164, Plenum, New York.

Wells, A. J., J. S. Wettlaufer, and S. A. Orszag (2011), Brine fluxes from growing sea ice, *Geophys. Res. Lett.*, *38*, L04501, doi:10.1029/2010GL046288.

Wiese, M., P. Griewank, and D. Notz (2015), On the thermodynamics of melting sea ice versus melting freshwater ice, *Annals of Glaciology*, *56 (69)*, 191–199.

Wieser, M. (2006), Atomic weights of the elements 2005 (IUPAC Technical Report), *Pure and Applied Chemistry*, *78*, 2051–2066.

Worster, M. G. (1992), *Interactive Dynamics of Convection and Solidification*, chap. The dynamics of mushy layers, pp. 113–138, Kluwer.

Zubov, N. N. (1945), *Arctic ice (in Russian)*, 217 pp. pp., U. S. Naval Oceanographic Office Translation.

Table 1. Precipitating minerals in FREZCHEM 13.3, along with their highest temperature of occurence and their mass fraction of total salt f_{sm} at the eutectic temperature ($T_e = -36.2°C$). $f_{sm}(T_e)$ is expressed as the mass of non-H_2O species within the considered mineral divided by the total mass of sea salt in the considered unit mass. FREZCHEM was run with standard seawater (*Millero et al.*, 2008), from 0°C down to −36.2°C, using 0.1°C steps.

Mineral	Formula	T (°C)	$f_{sm}(T_e)$ (%)
Ikaite	$CaCO_3 \cdot 6\,H_2O$	-4.9	0.2
Gypsum	$CaSO_4 \cdot 2\,H_2O$	-6.2	3.6
Mirabilite*	$Na_2SO_4 \cdot 10\,H_2O$	-6.4	0
Hydrohalite	$NaCl \cdot 2\,H_2O$	-22.9	75.4
Sodium Bromide	NaBr	-22.9	0.04
Meridianite	$MgSO_4 \cdot 11\,H_2O$	-33.3	6.2
Sylvite	KCl	-33.4	1.1
Magnesium chloride dodecahydrate	$MgCl_2 \cdot 12\,H_2O$	-36.2	13.5

* Mirabilite reaches a maximum $f_{sm} = 10.5\%$ at -22.9°C but dissolves back at lower temperature (*Marion et al.*, 1999).

Table 2. Main characteristics of the observational data sets used in this work. N is the number of relevant observations available.

Source	ΔT [K]	ΔS [g/kg]	T-range [°C]	S-range [g/kg]	Seawater type	N
			Liquidus salinity			
G37	0.1	< 0.1	$[-35.5, -1.8]$	$[32.8, 248.4]$	Synthetic	16
NT54*	0.05	< 0.1	$[-43.2, -4.4]$	$[70.8, 237.8]$	Pacific	9
DK74	2×10^{-3}	0.02	$[-2.2, -0.39]$	$[6.97, 40.2]$	Sargasso Sea	21
B16b	0.1	< 0.1	$[-20.6, -1.8]$	$[35.2, 218.7]$	Simplified	18
			Mirabilite			
B16a	0.1	n.a.	$[-6.4, -22.9]$	$[34.9, 225.9]$	Simplified	n.a.
			Liquid H_2O fraction			
RK66	0.5	0.001	$[-2, -42]$	$[10.022, 35.035]$	unspecified	23

G37 = *Gitterman* (1937), NT54 = *Nelson and Thompson* (1954), DK74 = *Doherty and Kester* (1974), B16a = *Butler et al.* (2016a), B16b=*Butler et al.* (2016b), RK66=*Richardson and Keller* (1966)

*Of the *Nelson and Thompson* (1954), only samples with reported SO_4^{2-} concentrations were retained.

Table 3. Liquidus computation methods used in this work.

Label	Computation methods	Reference
A58	$S_{br} = -18.4809\ T$	*Assur* (1958)
NW09	$S_{br} = -21.4\ T - 0.886\ T^2 - 0.0170\ T^3$	*Notz and Worster* (2009)
POLY3	$S_{br} = -18.7\ T - 0.519\ T^2 - 0.00535\ T^3$	This study (§2.3.1)
CW86	$S_{br} = \alpha_0 + \alpha_1\ T + \alpha_2\ T^2 + \alpha_3\ T^3$	*Cox and Weeks* (1986)
	$\alpha = [-3.9921, -22.700, -1.0015, -0.019956]$ $(-2 \geq T > -22.9°\text{C})$	
	$= [206.24, -1.8907, -0.060868, -0.0010247]$ $(-22.9 \geq T > 44°\text{C})$	
	$= [-4442.1, -277.86, -5.501, -0.03669]$ $(-44 \geq T > -54°\text{C})$	
mTEOS-10	$\Delta\mu^{TEOS-10}(S_{br}, T) + \mu^c(S_{br}) = 0$	This study (Appendix A)

Table 4. Evaluation of the liquidus curve $S_{br}(T)$ from selected computation methods, by comparison with the observational data (*Gitterman*, 1937; *Doherty and Kester*, 1974; *Butler et al.*, 2016b; *Nelson and Thompson*, 1954, Table 1), see Section 2.3.1 for details. The comparison is performed both for the entire temperature range (N=64) and for the TEOS-10 validity range ($T \geq -6$°C, $S \leq 120$ g/kg, N=29).

Type	Eutectic compliant?	Bias	RMSE	STDE	ΔS_e [g/kg]	Bias	RMSE	STDE
		Full T-range				TEOS-10 validity range		
FREZCHEM	No	1.1	1.9	2.5	3.4	0.08	0.5	1.15
Linear (A58)	No	75.6	75.6	109.3	418.4	1.67	1.80	3.50
3^{rd} order (NW09)	No	11.7	12.3	29.8	169.5	2.57	2.57	1.26
3^{rd} order (POLY3)	Yes	-0.4	2.3	3.2	0	-1.33	1.46	1.47
3^{rd} order piecewise (CW86)	No	1.2	2.9	3.5	-7.1	0.8	1.29	1.67
mTEOS-10	Yes	1.2	3.0	4.6	-0.007	0.04	0.6	1.14

ΔS_e: Difference between predicted $S_{br}(T_e)$ at the assumed eutectic temperature (-36.2°C) and the observational best estimate of the eutectic salinity (250.6146 g/kg). RMSE = Root mean square error, STDE = Standard deviation of error. A58 = *Assur* (1958), NW09 = *Notz and Worster* (2009), POLY3 = 3^{rd} polynomial (eq. 10), CW86 = *Cox and Weeks* (1986), mTEOS-10 = modified TEOS-10 (Section 2.4).

Table 5. Evaluation of liquid H_2O mass fraction (g/kg) retrieved from equation (4) with brine mass fraction computed based on equation (3), itself fed by various liquidus salinity and solid salt fraction estimates. Evaluation is performed by comparison with NMR-based estimates (*Richardson and Keller*, 1966, N=20), using the experimentally imposed temperatures and absolute salinities as a basis for computations.

Liquidus	Sol. salt frac.	Liquid frac.	Bias	RMSE	STDE
S_{br}	f_{sm}	ϕ_{br}	g/kg	g/kg	g/kg
FREZCHEM direct estimate of liquid H_2O fraction			1.1	8.6	13.3
FREZCHEM	FREZCHEM	n.a.	1.3	8.6	13.4
Linear (A58)	0	n.a.	-28.8	28.9	21.3
3^{rd} order (NW09)	0	n.a.	6.7	18.05	23.6
3^{rd} order (POLY3)	0	n.a.	20.3	20.7	19.4
3^{rd} order (POLY3)	FREZCHEM	n.a.	6.6	10.3	17.5
mTEOS-10	FREZCHEM	n.a.	-0.09	8.9	13.5
3^{rd} order piecewise (CW86)	n.a.*	CW83	-8.1	10.5	12.4

A58 = *Assur* (1958); NW09 = *Notz and Worster* (2009); POLY3 = 3^{rd} order observational fit (eq. 10); CW86 = *Cox and Weeks* (1986). CW83 = *Cox and Weeks* (1983).

* Here eq. 4 is fed directly by brine mass fraction. CW83 originally provide brine volume fraction, which is first converted into liquid mass fraction using eq. 5, using CW86 for liquidus salinity.

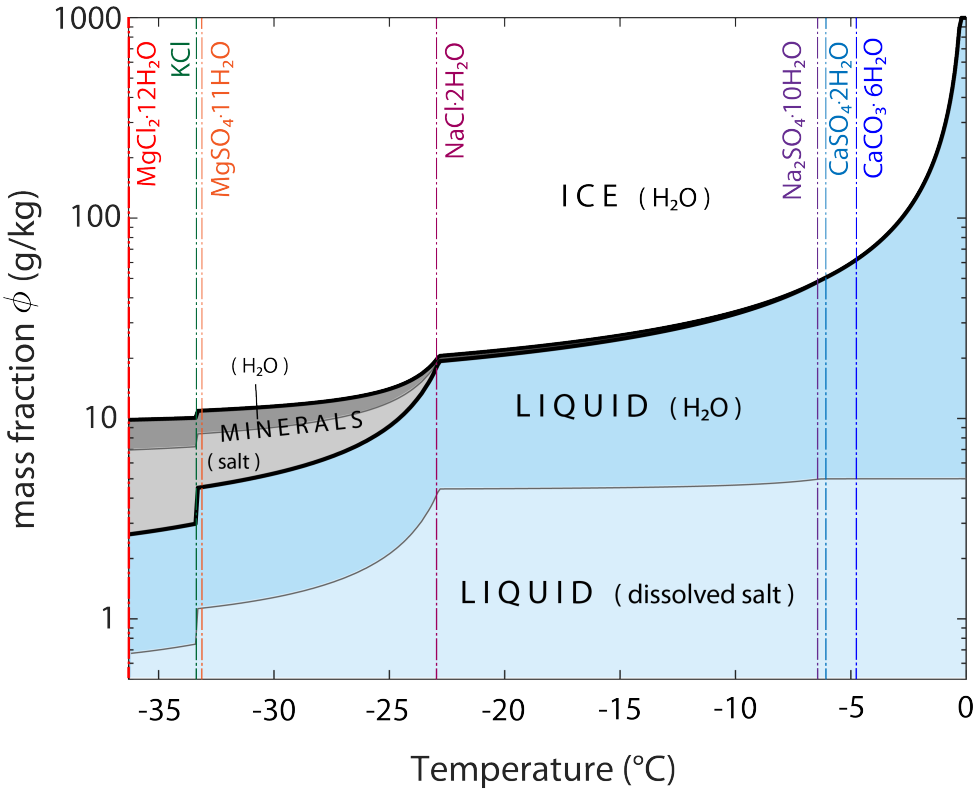

Figure 1. Sea ice phase diagram derived from FREZCHEM outputs, for sea ice with a typical absolute bulk salinity value of S=5 g/kg and standard seawater composition (*Millero et al.*, 2008). The mass fraction of the main sea ice constituents (following eq. 7) are shown cumulatively over the $[-36.2, 0°\mathrm{C}]$ temperature range. From bottom to top the lines refer to ϕ_{br}^{salt}, ϕ_{br}^{salt} $+\phi_{br}^{\mathrm{H_2O}}$, etc... and so the individual mass fractions are to be read as the vertical interval between the lines. The thick black lines separate individual phases (liquid, minerals, ice), whereas the thin grey lines further split salt and H_2O contributions. Note the logarithmic scale for the y-axis. fThe supplementary netcdf file includes data for the entired explored salinity range.

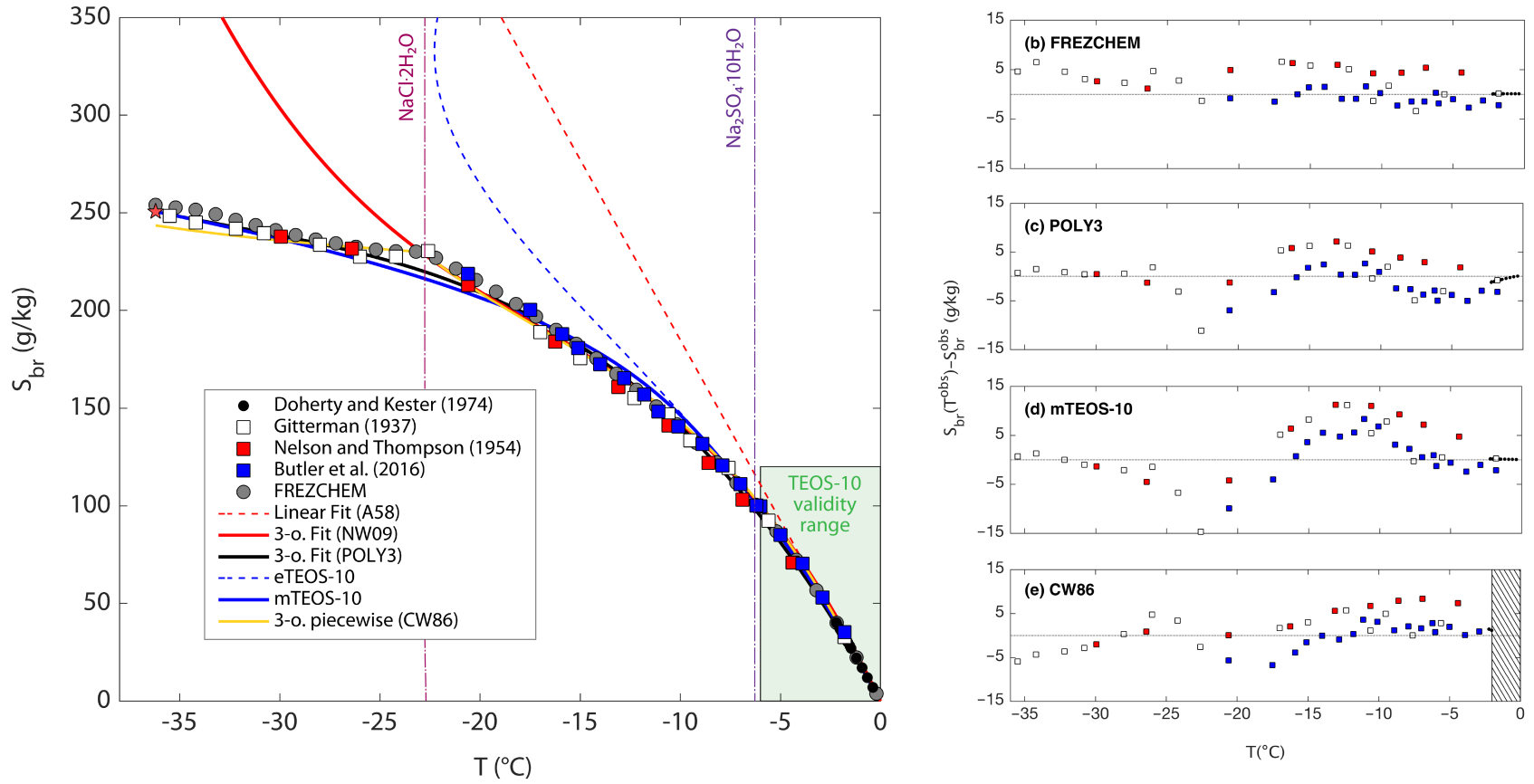

Figure 2. (a) Liquidus salinity as a function of ambient temperature from the Pitzer-Gibbs model (FREZCHEM, grey circles), other computational methods (lines) and observational sources (symbols). The eutectic point is represented by the red star. (b-e) Differences between calculated and observed liquidus salinity for the main computational methods discussed in the text. A58 = *Assur* (1958), NW09 = *Notz and Worster* (2009), POLY3 = 3^{rd} polynomial (eq. 10), eTEOS-10 = extended TEOS-10, mTEOS-10 = modified TEOS-10 (Section 2.4), CW86 = *Cox and Weeks* (1986).

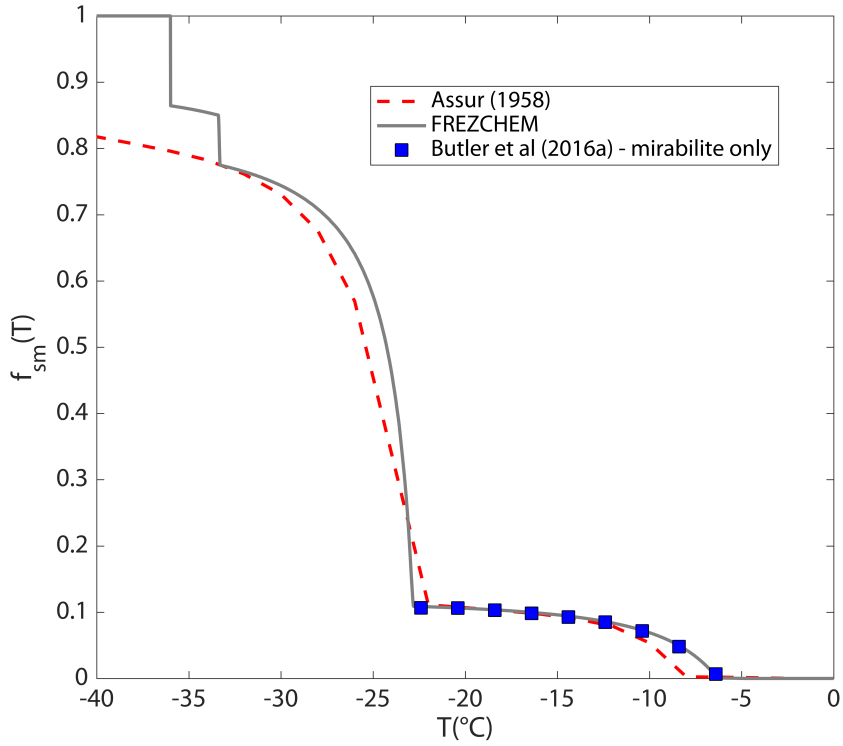

Figure 3. Solid salt fraction f_{sm} derived from FREZCHEM outputs, plotted against (i) the observational fit to the laboratory observations of *Butler et al.* (2016a) (their Table 4, only mirabilite included) and (ii) from the calculations of *Assur* (1958, derived from his Table 3).

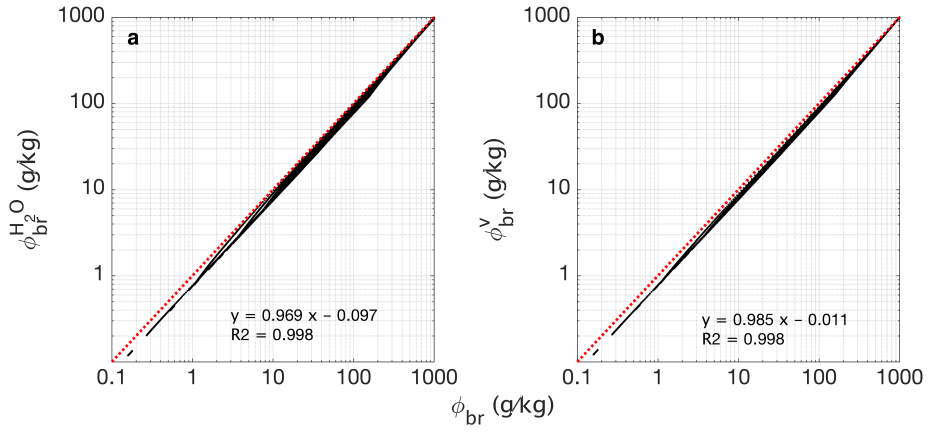

Figure 4. (a) Liquid H_2O mass fraction ($\phi_{br}^{H_2O}$) and (b) liquid volume fraction (ϕ_{br}^{v}) from the 41×363 points of the FREZCHEM outputs, plotted against mass fraction (ϕ_{br}). The red dots give the 1:1 line.

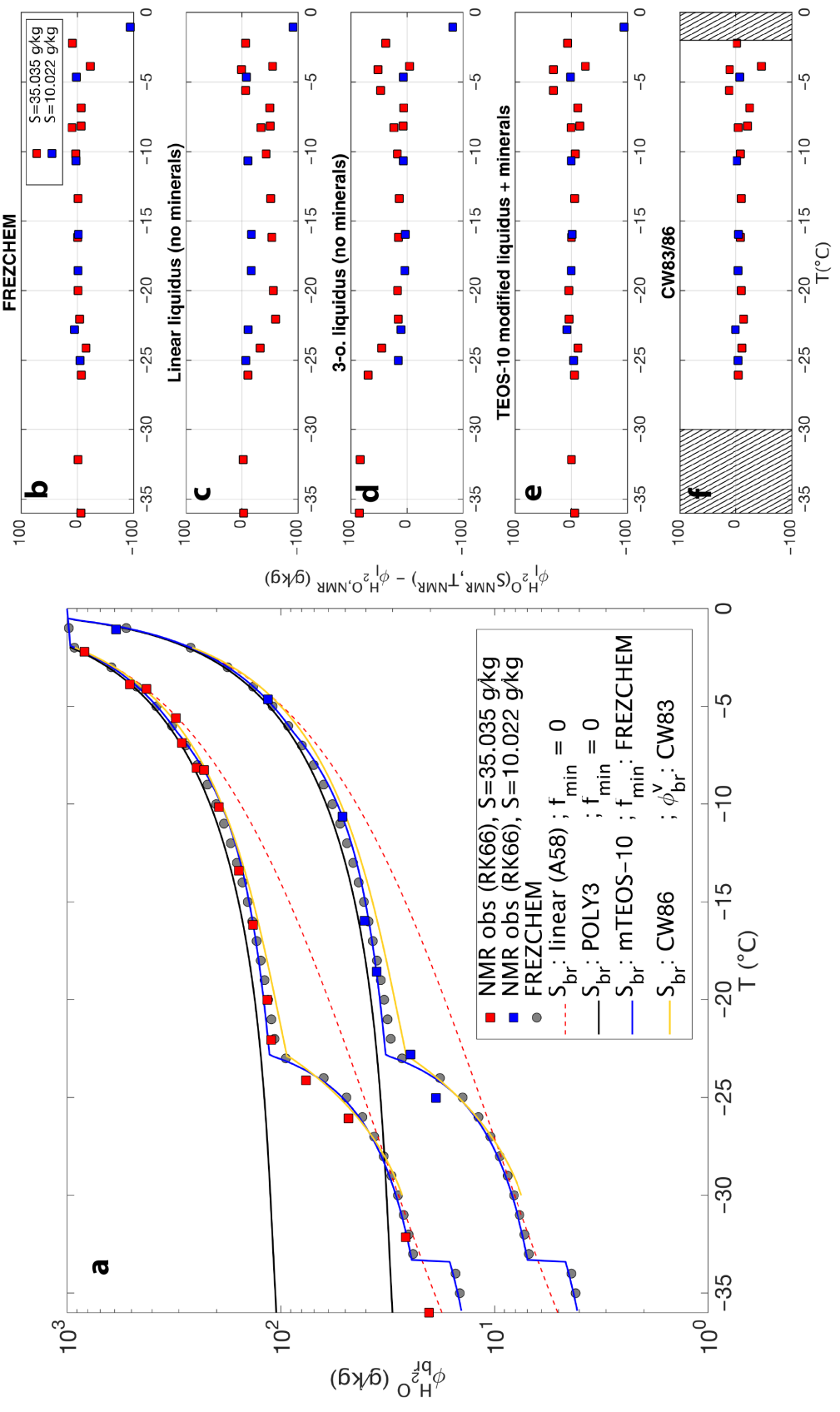

Figure 5. (Left) Liquid H_2O mass fraction as a function of ambient temperature from the Pitzer-Gibbs model (FREZCHEM, grey circles), other computational methods (lines) and digitized Nuclear Magnetic Resonance (NMR) estimates (*Richardson and Keller*, 1966, RK66) (squares, their Figures 2 and 3), at two reference absolute salinities ($S = 10.022, 35.035$ g/kg). (Right) Differences between calculated and NMR-derived liquid H_2O fraction estimates from the same sources.

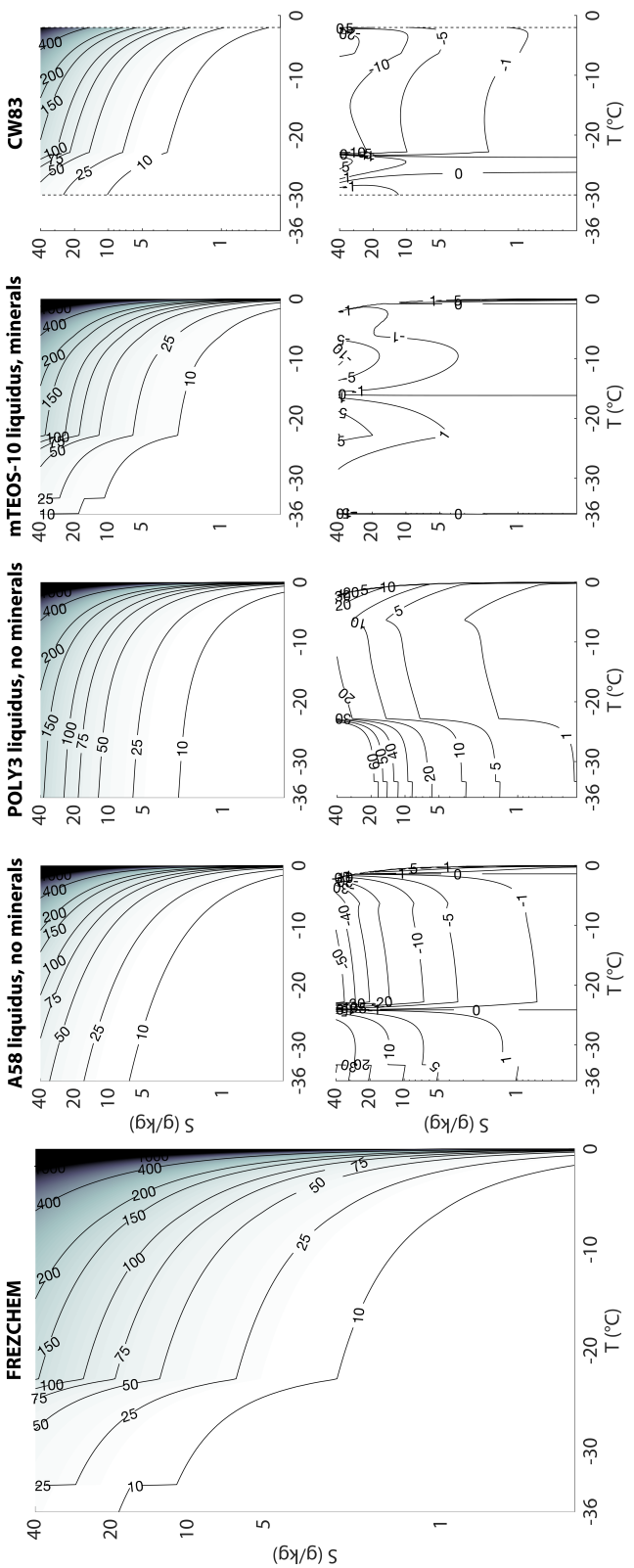

Figure 6. Liquid mass fraction contours in T-S space, derived from FREZCHEM outputs (left panel), from selected computational approaches (top panels), and differences of the latter with FREZCHEM (lower panels). CW83 refers to *Cox and Weeks* (1983) volume fraction converted into mass fraction using equation (5)

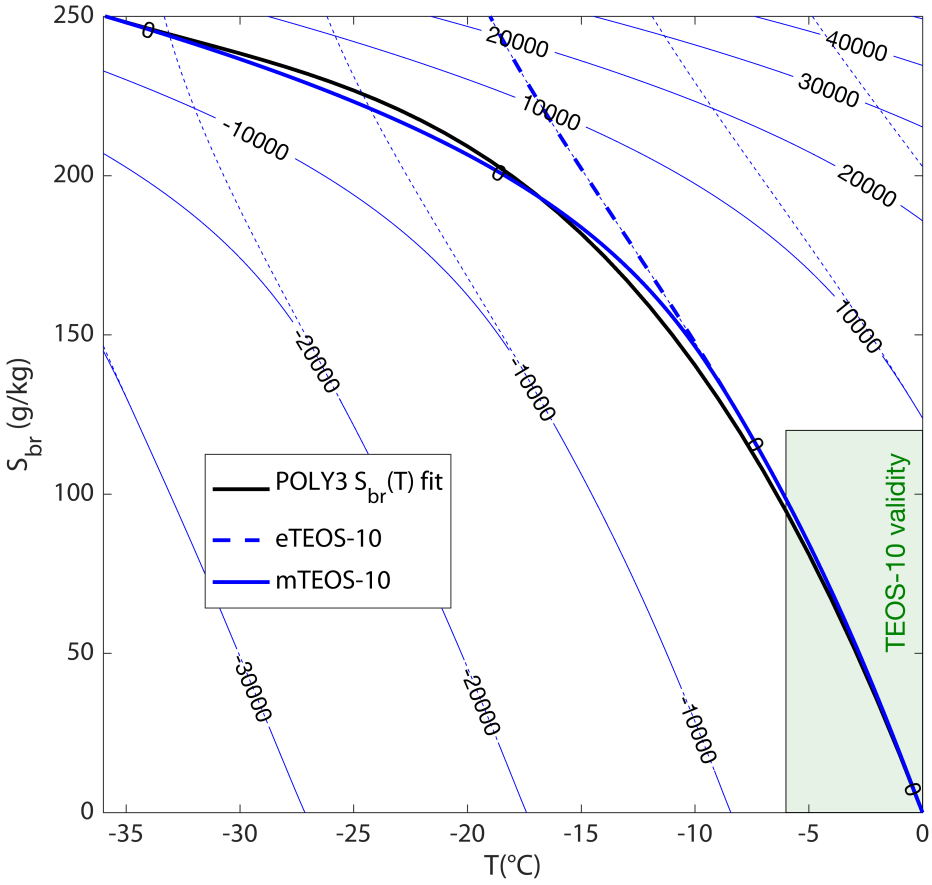

Figure A1. Why TEOS-10 liquidus differs from observations at high salinity and how can this be solved? Liquidus salinities from the POLY3 fit on observations (thick black line), the extended TEOS-10 (thick blue dotted line) and modified TEOS-10 (thick blue line) formulations. The background thin lines contour $\mu^{Ih}(T)$-$\mu^{w}(S_{br}, T)$ at reference atmospheric pressure using the extended (blue dots) and modified (solid blue) TEOS-10 formulations for the chemical potential of water in salt water. These give a more general context: positive contour values indicate that salt water is more stable than ice, whereas the zero contour corresponds to the liquidus curve.

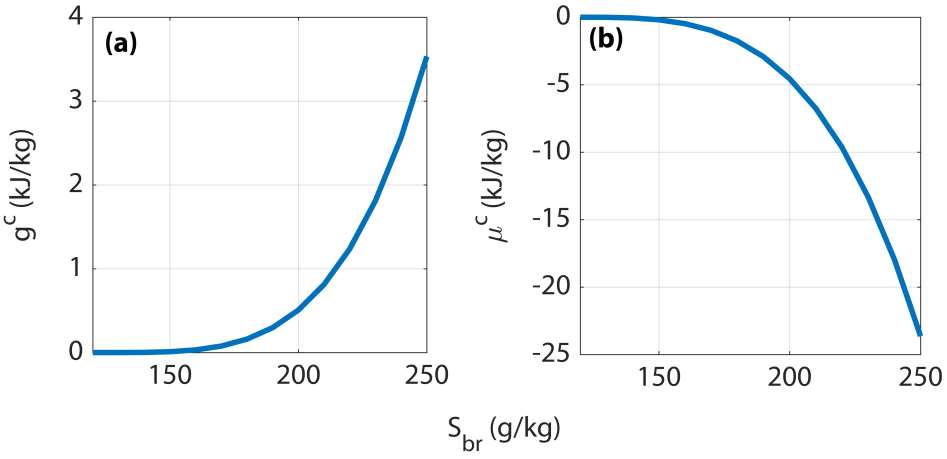

Figure A2. Perturbation functions to the seawater Gibbs free energy g^c=ax^4 and to the chemical potential of water in sea water $\mu^c = -3ax^4 - 4aS^0x^3$.

A Appendix: A liquidus curve consistent with TEOS-10

A.1 Why does using TEOS-10 beyond its limits not work?

Ocean models (e.g. *Madec and the NEMO team*, 2008) have recently been updated so that their thermodynamic properties – including the freezing temperature of seawater – all derive from the international thermodynamic equation of seawater (TEOS-10, *IOC, SCOR and IAPSO*, 2010). Using a fit to retrieve brine salinity as a function of temperature would always somehow conflict with such an approach, leading to inconsistencies between the freezing point of saline inclusions within sea ice and that of the seawater below.

Let us give an example. The freezing temperature T_{fr} obtained from the numerical inversion of the 3^{rd} order fit given by eq. 10 at a salinity of 35 g/kg is -1.978°C. (The numerical inversion is the most efficient approach we found, reaching a precision of 10^{-14} °C in a few iterations). At the same absolute salinity of 35 g/kg and at standard atmospheric pressure, TEOS-10 predicts $T_{fr} = -1.910$°C, that is 0.068°C higher. The difference is small, but may lead to situations where the ocean would see freezing seawater, whereas the sea ice model would assume that at such temperature, the medium should be all liquid. The inconsistency reaches 0.10°C with the *Cox and Weeks* (1986), and 0.15°C with the *Notz and Worster* (2009) fits.

Next to inconsistencies, another argument in support of TEOS-10 is intrinsic quality. Over its claimed validity range (T>=-6°C, S<120 g/kg), the TEOS-10 derived freezing point and liquidus salinity clearly outperform any other estimate. Indeed, as compared with the observational estimates (Section 2.3.1) lying within the TEOS-10 validity range ($N = 29$), the TEOS-10 liquidus salinity error is of 0.6 ± 1.1 g/kg, at least twice as small as any of the usual fits (see Table 4). TEOS-10 not only better fits the observations of *Doherty and Kester* (1974) over which it was fitted, but also the independently acquired data of *Gitterman* (1937) and *Butler et al.* (2016b). There is no retained observation from *Nelson and Thompson* (1954) falling within the TEOS-10 validity range.

Hence, to achieve consistency with ocean models and the best precision near the freezing point, the best approach to retrieve the liquidus salinity as a function of tem-

perature is to invert the TEOS-10 freezing point. However, out of its claimed validity range, the TEOS-10 freezing point has not been tested, and is by default undefined.

One can remove all the TEOS-10 high salinity and low temperature barriers to get a defined value for T_{fr} out of the claimed TEOS-10 validity bounds (an approach that we refer to as *extended* TEOS-10, illustrated with the dashed blue curve in Fig. A1). Yet, doing this brings two other problems. The first one, somehow expected, is that the resulting freezing temperature value rapidly departs from observations at salinities higher than 120 g/kg. The other problem is worse: the freezing temperature non-monotonically depends on temperature: the extended TEOS-10 freezing temperature reaches a minimum near approximately -22.3°C near $S = 330$ g/kg and then increases back to warmer temperatures . This non-monotonicity implies that the reciprocal of the TEOS-10 freezing temperature, i.e., the liquidus salinity, is undefined below -22.3°C. For this reason, the extended TEOS-10 approach is not workable and must be rejected.

A.2 What should be modified in TEOS-10?

The desire to achieve a precise estimate of the liquidus salinity at all temperatures, fully consistent with ocean models, encouraged us to seek a modification of TEOS-10 that would ensure a reasonable freezing temperature out of its claimed validity bounds. To do this, we must first explain how TEOS-10 derives the freezing temperature as a function of salinity. Let us mention that all salinities are absolute in the TEOS-10 sense, that temperatures are expressed in Celsius, and that pressure effects are ignored in the following developments.

The TEOS-10 approach is based on a complete specification of the state of a unit mass of seawater by the Gibbs free energy or potential in J/kg. The Gibbs potential is an extensive variable; and therefore the sea ice Gibbs function g can be written as the sum of pure ice of Ih crystal type (g^{Ih}) and salt water (g^{sw}) contributions weighted by brine fraction ϕ_{br} (*Feistel and Hagen*, 1998):

$$g(\phi_{br}, S_{br}, T) = g^{Ih}(T)(1 - \phi_{br}) + g^{sw}(S_{br}, T)\phi_{br}, \tag{A.1}$$

a form that assumes a negligible contribution of minerals to the Gibbs function. The TEOS-10 manual and routines provide exhaustive polynomial developments for the seawater Gibbs potential g^{sw} (*Feistel*, 2008), and also provide the IAPWS Gibbs potential for ice *Ih*, g^{Ih} (*Feistel and Wagner*, 2006). The equilibrium of liquid and solid phases occurs

at the minimum of the Gibbs function ($\partial g/\partial\phi = 0$), or equivalently at equal chemical potentials for pure ice and water in salt water (*Feistel and Hagen*, 1998). The liquidus curve $S_{br}(T)$ (and the freezing temperature $T_f(S)$) stems from the equality of the chemical potentials and therefore verifies:

$$\Delta\mu(S_{br}, T) \equiv \mu^{Ih}(T) - \mu^{w}(S_{br}, T) = 0, \tag{A.2}$$

where μ^{Ih} and μ^{w} are the chemical potentials of ice *Ih* and water in salt water, respectively, and $\Delta\mu$ is defined as the difference between both. Using the relations between chemical and Gibbs potentials for ice *Ih* ($g^{Ih} = \mu^{Ih}$) and of water in salt water ($\mu^{w} = g^{sw} - S \cdot \partial g^{sw}/\partial S$), the freezing condition becomes:

$$\Delta\mu(S_{br}, T) = g^{Ih}(T) - g^{sw}(S_{br}, T) + \left[S \cdot \frac{\partial g^{sw}}{\partial S} \right]_{S_{br},T} = 0. \tag{A.3}$$

It is from this expression of the freezing condition that the TEOS-10 freezing point is numerically derived, using the IAPWS-06 for g^{Ih} and TEOS-10 for g^{sw}.

Fig. A1 depicts the contours of $\Delta\mu$ in $T-S_{br}$ space, based on IAPWS-06 and TEOS-10 Gibbs potentials. We see that within the claimed validity range of TEOS-10 ($[-6, 40°\text{C}]$, $[0, 120$ g/kg$]$), the zero contour of $\Delta\mu$ (equivalent to the TEOS-10 freezing point) closely matches the observation-derived liquidus curve but spreads from it at high salinity. This mismatch suggests the need to modify the sea ice Gibbs function and the associated chemical potentials in such a way that the zero contour of $\Delta\mu$ gets closer to the observed liquidus curve. We argue that it is TEOS-10 that should be modified, not IAPWS-06, because the latter has been tested over a much wider temperature range than TEOS-10 and has no salinity dependence anyway.

A.3 Modifying TEOS-10 to improve the freezing point at salinities higher than 120 g/kg.

We seek a modification of TEOS-10 modification that achieves two basic requirements:

- to preserve TEOS-10 integrity within its claimed validity range and,
- to give a liquidus curve in better agreement with observations at high salinity.

Such TEOS-10 modification should be done at the most fundamental level, namely by acting on the Gibbs function. We target the salinity dependency of g, because the lat-

ter determines the chemical potential of water in salt water. In addition, S must be the master independent variable for such operation because the extended TEOS-10 freezing point is not monotonic at high salinity.

On these grounds, we propose the following *modified* Gibbs function for salt water:

$$g^{sw}(S_{br}, T) = g^{TEOS-10}(S_{br}, T) + g^c(S_{br}), \tag{A.4}$$

where $g^c = g^c(S_{br})$ should be constructed such that the freezing condition [eq. A.3] fits the freezing temperature data $T_f^n(S_A^n)$, with n=1, ..., 31. To preserve TEOS-10 integrity, we only use the 31 data points in the ranges $S > 120$ g/kg and $T > -36.2°$C.

In order to derive a fitting function, we impose the freezing condition (eq. A.3) to hold along the expected freezing temperature $T_f(S_{br})$ curve. Re-expressing in terms of g^c, we get:

$$\mu^c \equiv g^c - S \cdot \frac{\partial g^c}{\partial S_{br}} = \Delta\mu^{TEOS-10}[S_{br}, T_f(S_{br})]. \tag{A.5}$$

where the right-hand side, only a function of S_{br}, is evaluated using the IAPWS-06 and extended TEOS-10 Gibbs potentials (unperturbed) for ice *Ih* and salt water. $\Delta\mu^{TEOS-10}$ is evaluated at the sought freezing point, not at the predicted freezing point, hence $\Delta\mu^{TEOS-10} \neq 0$. μ_c can be seen as the perturbation applied to the $TEOS{-}10$ chemical potential of water in salt water $\mu^w = \mu^{w,TEOS-10} + \mu^c(S_{br})$.

Now, as a practical matter, we want to only add this correction to the TEOS-10 Gibbs function when the absolute salinity is greater than the upper limit of the range of validity of the TEOS-10 Gibbs function, namely when $S_{br} > S_0 = 120$ g/kg. Let us define

$$x = S_{br} - S_0, \tag{A.6}$$

and we will seek a functional form for g^c as a polynomial in x. The freezing condition reads:

$$g^c - (x + S_0) \cdot \frac{\partial g^c}{\partial x} = \Delta\mu^{TEOS-10}(x) \tag{A.7}$$

We impose the two additional constraints:

$$\begin{aligned} g^c(x \leq 0) &= 0, \quad \text{(TEOS-10 integrity)}, \\ \left[g^c - (x + S_0) \cdot \tfrac{\partial g^c}{\partial x}\right]_{x_e = S_e - S_0} &= \Delta\mu[S_e, T_e(S_e)], \quad \text{(Eutectic compliance)}, \end{aligned} \tag{A.8}$$

with $S_e = 250.6146$ g/kg and $T_e = -36.2°$C are the eutectic salinity and temperature, respectively. On these grounds, one can fit a freezing point function $g^c(S)$ that sat-

isfies the two constraints and minimizes the least-square difference between μ^c and $\Delta\mu(S^n, T_f^n)$, n=1-31 (see Fig. S1 for an example). From μ_c, a *modified* TEOS-10 freezing point can then be obtained by solving $\mu_w[S_{br}, T_f(S_{br})] = \mu_i[T_f(S_{br})]$, and the liquidus curve $S_{br}(T)$ can be retrieved by numerical inversion.

We tried several forms for the Gibbs perturbation function g^c. For instance, we tried $g^c(x) = ax^2 + bx^3 + cx^4$, and computed the coefficients by minimizing the square difference between μ^c and $\Delta\mu$ and ensuring that the two constraints [A.8] were respected, giving a liquidus curve in very good agreement with observations ($\Delta S_{br} = 2.8 \pm 4.4$ g/kg). Relieving the eutectic compliance implies a lower brine salinity bias overall, but implies errors on eutectic temperature of about 3°C.

The most convenient expression we could find takes the following quartic form:

$$g^c(x) = a \cdot x^4, \quad a = 1.2370 \times 10^{-5} \text{ J/kg/(g}^4\text{/kg}^4\text{)} \tag{A.9}$$

depicted in Fig. A2 (together with the chemical potential perturbation function). The quartic form does virtually as well ($\Delta S_{br} = 3.0 \pm 4.6$ g/kg) as more complicated attempts. Such quartic expression is convenient for several reasons. First it is simple. Second, the coefficient a does not need to be fitted, it rather direclty derives from the eutectic compliance condition. Third, the S_{br} derivatives of the full Gibbs function are continuous up to order 3 at $x = 0$. g^c changes the freezing condition in a way that appropriately curves the freezing point function ($\Delta\mu = 0$ isoline) at high salinities (Fig. A1).